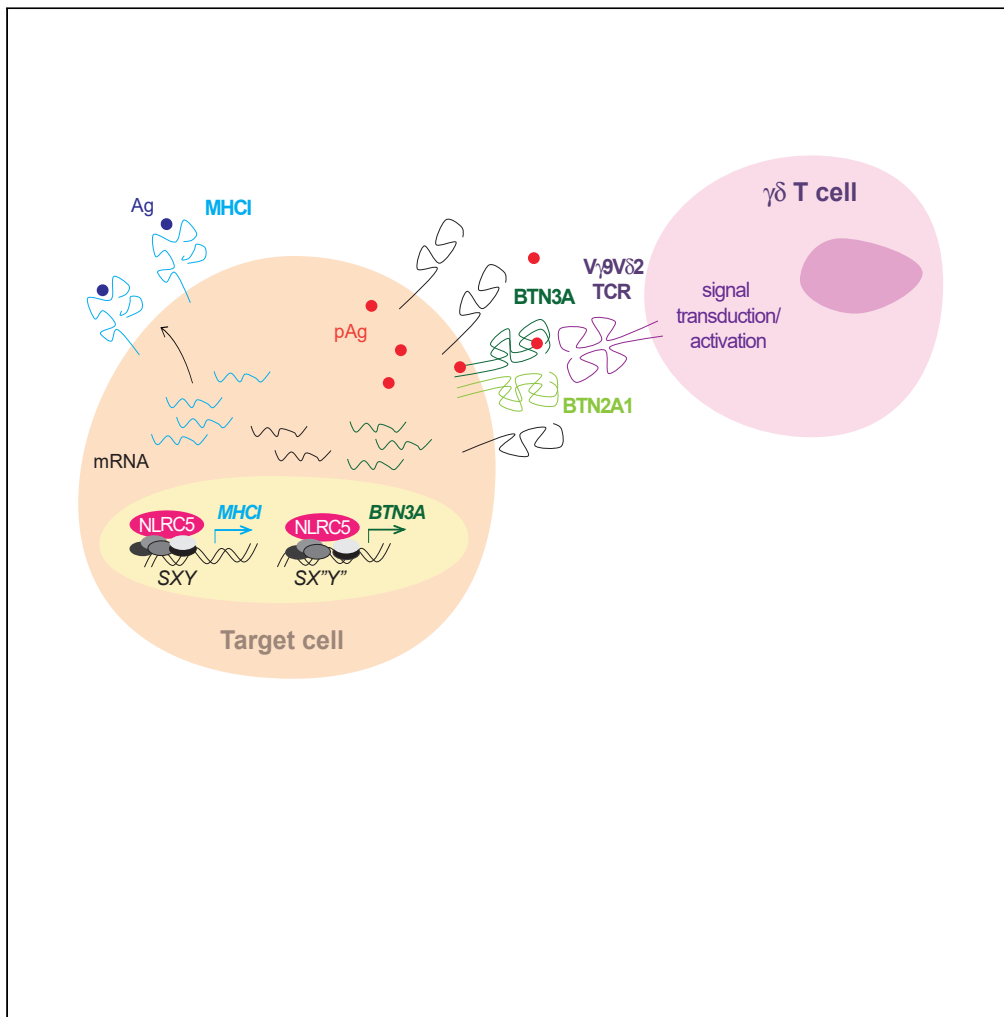


Article

NLRC5 promotes transcription of *BTN3A1-3* genes and $V\gamma 9V\delta 2$ T cell-mediated killing

Anh Thu Dang,
Juliane Strietz,
Alessandro
Zenobi, ..., Susana
Minguet, Sonia T.
Chelbi, Greta
Guarda

sonia.chelbi@irb.usi.ch (S.T.C.)
greta.guarda@irb.usi.ch (G.G.)

HIGHLIGHTS

BTN3A promoters contain a unique regulatory motif occupied by overexpressed NLRC5

NLRC5 and *BTN3A* mRNA levels correlate in healthy and diseased cells

NLRC5 overexpression increases susceptibility to $V\gamma 9V\delta 2$ T-cell-mediated elimination

Article

NLRC5 promotes transcription of *BTN3A1-3* genes and V γ 9V δ 2 T cell-mediated killing

Anh Thu Dang,^{1,10} Juliane Strietz,^{2,3} Alessandro Zenobi,⁴ Hanif J. Khameneh,⁴ Simon M. Brandl,^{2,3,5} Laura Lozza,⁶ Gregor Conradt,^{2,3} Stefan H.E. Kaufmann,^{6,7} Walter Reith,⁸ Ivo Kwee,⁴ Susana Minguet,^{2,3,9} Sonia T. Chelbi,^{4,*} and Greta Guarda^{4,11,*}

SUMMARY

BTN3A molecules—BTN3A1 in particular—emerged as important mediators of V γ 9V δ 2 T cell activation by phosphoantigens. These metabolites can originate from infections, e.g. with *Mycobacterium tuberculosis*, or by alterations in cellular metabolism. Despite the growing interest in the *BTN3A* genes and their high expression in immune cells and various cancers, little is known about their transcriptional regulation. Here we show that these genes are induced by NLRC5, a regulator of MHC class I gene transcription, through an atypical regulatory motif found in their promoters. Accordingly, a robust correlation between NLRC5 and *BTN3A* gene expression was found in healthy, in *M. tuberculosis*-infected donors' blood cells, and in primary tumors. Moreover, forcing NLRC5 expression promoted V γ 9V δ 2 T-cell-mediated killing of tumor cells in a *BTN3A*-dependent manner. Altogether, these findings indicate that NLRC5 regulates the expression of *BTN3A* genes and hence open opportunities to modulate anti-microbial and anticancer immunity.

INTRODUCTION

Butyrophilins (BTNs) are an emerging family of molecules fulfilling immune and non-immune functions. Human BTNs comprise BTN1A1, BTN2A1, and BTN2A2, as well as BTN3A1, BTN3A2, and BTN3A3. The genes encoding these proteins are located in the extended major histocompatibility complex (MHC) locus on chromosome 6 (Abeler-Dorner et al., 2012; Arnett and Viney, 2014). Structurally, BTNs are membrane proteins sharing similarity with the B7 immunoglobulin superfamily of costimulatory/coinhibitory molecules (Arnett and Viney, 2014). In fact, BTN2A2 and BTN1A1 have been shown to act as co-inhibitory ligands hindering T cell activation and proliferation, and *Btn2a2* knockout mice exhibit exacerbated T-cell-mediated autoimmunity (Sarter et al., 2016; Smith et al., 2010).

Human *BTN3A1-3* proteins, which have no murine homologs, are composed of two extracellular immunoglobulin-like domains and a transmembrane region linked—in *BTN3A1* and *BTN3A3*—to an intracellular B30.2 domain (Harly et al., 2012; Sandstrom et al., 2014; Vavassori et al., 2013). Despite this divergence in the intracellular portion, *BTN3A1*, *BTN3A2*, and *BTN3A3* show >95% homology in the extracellular domain, suggesting that they are the products of recent duplications. Although not sufficient, *BTN3A1* is necessary for the activation of V γ 9V δ 2 T cells (Riano et al., 2014; Sandstrom et al., 2014; Vantourout et al., 2018; Vavassori et al., 2013). Although the expression of *BTN3A2* and *BTN3A3* can support *BTN3A1*'s function, it recently became clear that *BTN2A1* is the second critical molecule to stimulate V γ 9V δ 2 T cells (Karunakaran et al., 2020; Rigau et al., 2020; Vantourout et al., 2018). *BTN2A1* presents the intracellular B30.2 domain and the two extracellular immunoglobulin-like domains (Abeler-Dorner et al., 2012; Arnett and Viney, 2014). V γ 9V δ 2 T cells are activated by phosphorylated metabolites, also called phosphoantigens (PAGs), that derive from a dysfunctional mevalonate pathway, such as isopentenyl pyrophosphate (IPP), or from microorganisms, as for instance *Mycobacterium tuberculosis*-derived (E)-4-hydroxy-3-methyl-but-2-enyl pyrophosphate (HMBPP) (Vantourout and Hayday, 2013). PAGs have been proposed to bind either the immunoglobulin-like domain or the B30.2 domain of *BTN3A1*, inducing a conformational change and/or stabilizing surface *BTN3A1* to engage the $\gamma\delta$ T cell receptor, whereas *BTN2A1* interacts with the germline region of the V γ 9 chain (Gu et al., 2017; Harly et al., 2012; Karunakaran et al., 2020; Rigau et al., 2020; Sandstrom et al., 2014; Vavassori et al., 2013). Increased levels of PAGs from metabolically stressed,

¹Department of Biochemistry, University of Lausanne, 1066 Epalinges, Switzerland

²Department of Immunology, Faculty of Biology, University of Freiburg, 79104 Freiburg, Germany

³Signalling Research Centres BIOSS and CIBSS, University of Freiburg, 79104 Freiburg, Germany

⁴Università della Svizzera italiana (USI), Faculty of Biomedical Sciences, Institute for Research in Biomedicine, 6500 Bellinzona, Switzerland

⁵Spemann Graduate School of Biology and Medicine (SGBM), Albert-Ludwigs-University Freiburg, 79104 Freiburg, Germany

⁶Department of Immunology, Max Planck Institute for Infection Biology, Berlin 10117, Germany

⁷Hagler Institute for Advanced Study at Texas A&M University, College Station, TX 77843, USA

⁸Department of Pathology and Immunology, University of Geneva Medical School, 1211 Geneva, Switzerland

⁹Center for Chronic Immunodeficiency (CCI), Medical Center - University of Freiburg, Faculty of Medicine, University of Freiburg, 79106 Freiburg, Germany

¹⁰Present address: Department of Immunology and Pathology, Monash University, Melbourne, Australia

¹¹Lead Contact

*Correspondence: sonia.chelbi@irb.usi.ch (S.T.C.), greta.guarda@irb.usi.ch (G.G.)

<https://doi.org/10.1016/j.isci.2020.101900>



transformed, and infected cells are thus sensed by V γ 9V δ 2 T cells, leading to their activation, expansion, and participation in the immune response (De Libero et al., 2014). For instance, this subset of unconventional T cells is significantly expanded during *M. tuberculosis* infection (Cheng et al., 2018; Kabelitz et al., 1991). Furthermore, intratumoral $\gamma\delta$ T cells emerged as the most significant favorable cancer-wide prognostic population, and their potential role in immunotherapy is being increasingly investigated (Benyamine et al., 2016, 2017; Gentles et al., 2015; Le Page et al., 2012; Peedicayil et al., 2010; Zocchi et al., 2017).

The transcriptional regulation of *BTN* genes remains poorly characterized. Recently, it has been shown that *Btn2a2* induction is regulated by the transcriptional regulator CIITA (class II major histocompatibility complex transactivator) (Sarter et al., 2016). This factor belongs to the nucleotide-binding oligomerization domain (NOD)-like receptor (NLR) family of proteins and, together with its closest homolog NLRC5 (NLR family CARD domain containing 5), is known to control the transcription of MHC and related genes (Chelbi et al., 2017; Jongsma et al., 2019; Reith and Mach, 2001; Sarter et al., 2016). CIITA is the master transcriptional regulator of MHC class II genes, whereas we and others showed that NLRC5 is an important transcriptional regulator of MHC class I genes, markedly in T lymphocytes (Chelbi et al., 2017; Meissner et al., 2010; Neerincx et al., 2013; Robbins et al., 2012; Staehli et al., 2012; Yao et al., 2012). These two NLRs, CIITA and NLRC5, are recruited to their respective target gene promoter by a multiprotein complex known as “enhanceosome” (Ludigs et al., 2015; Meissner et al., 2012a; Neerincx et al., 2012). This complex assembles on the promoter sequence called “SXY” module, which is composed of four individual elements (S, X₁, X₂, and Y) oriented and spaced in a specific manner (Anderson et al., 2017; Ludigs et al., 2015; Masternak et al., 2003; Meissner et al., 2012b; Neerincx et al., 2012 (Krawczyk et al., 2004)). Although we still do not know which factor recognizes the S-box, the X₁-box is bound by the regulatory factor X (RFX) complex, the X₂-box by cAMP-responsive element binding protein (CREB)/activating transcription factor (ATF) family members, and the Y-box by the nuclear transcription factor Y (NFY)-complex (Chelbi et al., 2017). Taken together, the finding that *Btn2a2* is a target of CIITA and the localization of *BTN* genes close to the MHC locus suggest the existence of common evolutionary links. This prompted us to investigate the transcriptional regulation of *BTN* genes and to hypothesize that they represent a novel set of NLRC5 or CIITA targets.

We found that *BTN3A1-3* genes exhibited an atypical SXY module in their proximal promoter region. This regulatory motif presented a reverse complement Y-box at an altered spacing from the X-motif. Using chromatin immunoprecipitation and gene reporter assays, we demonstrated that overexpressed NLRC5 occupies and transactivates this atypical module. We showed that forcing NLRC5 expression led to increased levels of *BTN3A* mRNA and protein. Data mining in transcriptome datasets of *M. tuberculosis*-infected and uninfected individuals' blood as well as of various cancers revealed a strong correlation between *NLRC5* and *BTN3A1* and *BTN3A2* gene expression. Furthermore, loss of both *NLRC5* copies was associated with significantly diminished expression of *BTN3A1* and *BTN3A2* in cancer cells. On a functional level, we observed that overexpression of NLRC5 enhanced V γ 9V δ 2 T-cell-mediated elimination of target cells, which was mediated by *BTN3A* molecules as demonstrated using a loss-of-function approach. Altogether, these findings indicate NLRC5 modulation as a possible way of targeting V γ 9V δ 2 T-cell-mediated immunity.

RESULTS

BTN3A genes have distinguishable S and X modules

To understand how far the mechanisms governing MHC gene transcription might be common to *BTN* genes, we screened their promoter sequences for the presence of SXY modules (Figures 1A and 1B) (Krawczyk et al., 2008; Ludigs et al., 2015). We confirmed the presence of an SXY consensus in the *BTN2A2* promoter (Figure 1B) (Sarter et al., 2016). Previous findings showed that the S-motif of NLRC5-occupied promoters is unique and strictly required for NLRC5 activity (Figure 1A) (Ludigs et al., 2015; Meissner et al., 2012a). The S-box sequence in both human and mouse *BTN2A2* did not suggest regulation through NLRC5, but rather a role for CIITA (Figures 1B and S1A). Indeed, expression of murine *Btn2a2* in various organs derived from *Nlrc5*-deficient mice was not significantly decreased (Figure S1A). We also noticed the presence of an X-motif in the promoters of *BTN2A1*, the pseudogene *BTN2A3*, *BTN3A1*, *BTN3A2*, and *BTN3A3* genes (Figures 1A and 1B). Of note, 15 bp upstream of the X-box, the highly homologous promoter regions of the *BTN3A* genes, exhibited an S-box suggestive of NLRC5-mediated transcriptional regulation.

BTN3A1-3, *BTN2A1*, *NLRC5*, and *CIITA* transcripts were abundant in most of the tested immune organs and cells (Figure 1C). Among the main blood cell subsets, the mRNA profile of *BTN3A1-3* was reminiscent

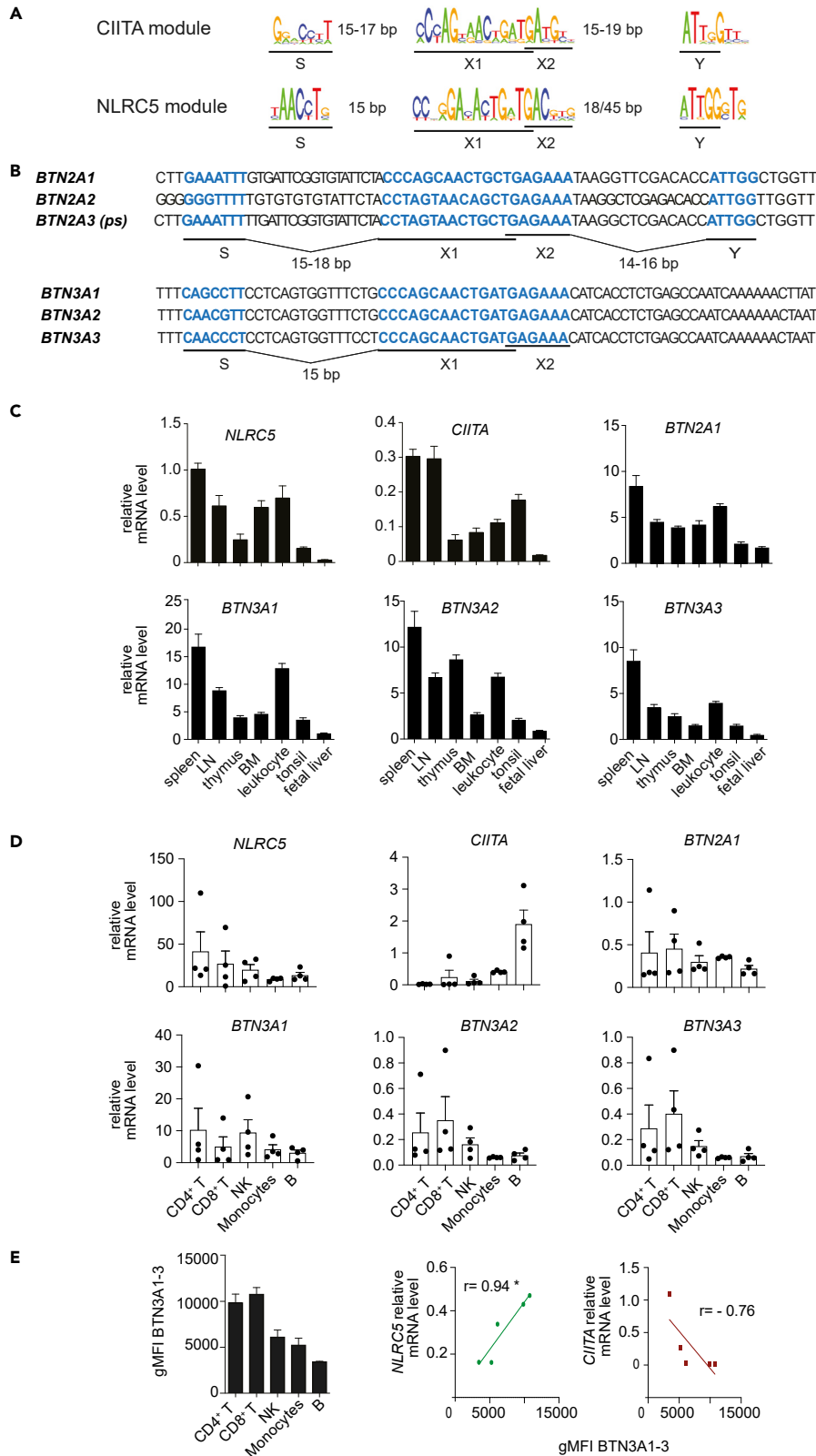


Figure 1. *BTN3A* promoters present conserved S- and X-boxes

(A) The sequence logo for the human *CIITA* and mouse *NLRC5* SXY consensus are shown.
 (B) Sequence alignment of the S-, X-, and Y-motifs located within the proximal promoter region of human *BTN2A1*, *BTN2A2*, *BTN2A3* (ps, pseudogene), *BTN3A1*, *BTN3A2*, and *BTN3A3* genes. The sequences corresponding to the S-, X-, and Y-motifs are highlighted in blue and distances between them are indicated.
 (C and D) *NLRC5*, *CIITA*, *BTN2A1*, and *BTN3A1-3* mRNA levels (relative to *POLR2A* mRNA) were assessed by quantitative RT-PCR (qRT-PCR) in the indicated human tissues (C) and in blood-derived CD4⁺ T cells (CD4⁺CD3⁺), CD8⁺ T cells (CD8⁺CD3⁺), NK cells (CD56⁺CD3⁻), monocytes (CD14⁺CD3⁻), and B cells (CD19⁺CD3⁻) (D).
 (E) Geometric mean fluorescence intensity (gMFI) of *BTN3A1-3* (CD277) as measured by flow cytometry in the indicated blood-derived cell subsets (on the left) and the correlation of the mean value with those of *NLRC5* and *CIITA* mRNA levels measured by qRT-PCR in the same cells (on the right). Spearman's correlation coefficient (R) and significance are indicated. (C–E) Results illustrate mean ± SD of n = 3 technical replicates (C) and mean ± SEM of n = 4 (D) and n = 3 (E) individual donors. Lymph node, LN; bone marrow, BM. *p < 0.05

of the one of *NLRC5*, whereas it largely differed from the one of *CIITA* (Figure 1D). Instead, *BTN2A1* presented a distinct pattern, characterized by higher expression levels in monocytes (Figure 1D) (Rigau et al., 2020). We also observed a marked similarity between the expression pattern of *NLRC5* and the *BTN3A* protein display (by using a monoclonal antibody anti-CD277, which recognizes all three *BTN3A* isoforms; Figures 1E and S1B). We next took advantage of bare lymphocyte syndrome (BLS) patient-derived and *in-vitro*-generated B cell lines lacking expression of *CIITA* or the RFX complex subunit RFX5 or RFXAP (Ludigs et al., 2015; Tarantelli et al., 2018). The absence of the RFX factors affected the expression of *BTN3A1-3* and *BTN2A1* transcripts, in particular following interferon (IFN) γ treatment (Figure S1C). This was not observed in the absence of *CIITA*, indicating that this NLR was not necessary for the regulation of these genes (Figure S1C). Taken together, these data support the involvement of the enhanceosome platform and prompted us to perform further analyses on *NLRC5* in the regulation of *BTN3A1-3* genes.

NLRC5 overexpression induces transcription of *BTN3A* genes

We next tested whether *NLRC5* induced the transcription of *BTN3A1-3* genes, first employing a primer pair that detects all three gene products. After 48 h, overexpression of *NLRC5* in HEK293T cells led to increased transcript levels of *BTN3A1-3* and *HLA-B*, the latter used here as a positive control (Figure 2A). To assess the specificity of the transcriptional effects of *NLRC5*, we overexpressed other NLR members. Although *NOD1*, *NOD2*, and *NLRC3* had marginal effects on the expression of *BTN3A1-3* and of *HLA-B*, two *CIITA* isoforms (*CIITA I* and *CIITA III*) induced the *BTN3A1-3* and the *HLA-B* gene (Figure 2A). The induction in the levels of *BTN3A1-3* and *HLA-B* transcripts by *NLRC5* and *CIITA I* encoding plasmids was already detected 24 h following transfection (Figure S2A). Both *NLRC5* and *CIITA I* induced the three *BTN3A* genes (Figure 2B). In contrast, only *CIITA I* moderately induced *BTN2A1* mRNA (Figure 2B). Finally, we demonstrated that overexpression of *NLRC5* and *CIITA*, but not of *NLRC3*, increased surface expression of *BTN3A1-3* (Figure 2C). It is important to point out that although *CIITA* does not regulate MHC class I genes at the endogenous level, it is well established that its overexpression leads to their transactivation (Chang et al., 1996; Gobin et al., 1997; Ludigs et al., 2015; Martin et al., 1997; Robbins et al., 2012; Williams et al., 1998), as shown for *HLA-B* (Figure S2B). Conversely, the activity of *NLRC5* maintains its specificity toward the *HLA-B* but not *HLA-DRA* genes even when overexpressed (Figure S2B). Therefore, these data encouraged us to further investigate whether *BTN3A1-3* genes are regulated by mechanisms similar to the ones controlling MHC class I gene expression.

***BTN3A* genes have an atypical SXY module**

In order to substantiate the hypothesis that *BTN3A1-3* are direct targets of *NLRC5*, we cloned the proximal promoter region, containing the S- and X-motif, of *BTN3A2*—as a representative *BTN3A* promoter—into a luciferase reporter plasmid (referred to as “SX”). As we did not identify an “ATTGG” Y-box sequence nearby, we hypothesized that it could be dispensable for *NLRC5*-dependent transactivation of these genes (Figure 1B). However, we observed that these promoters were not transactivated by *NLRC5* (Figure 3A). We therefore took a closer look at the promoters of *BTN3A1-3* genes and identified the reverse complement of the “ATTGG” Y-box, “CCAAT,” 13 bp downstream of the X-box (Figure 3B). As the latter constitutes the canonical NFY-binding site, we cloned an extended portion of the promoters, which included this motif, into a luciferase reporter plasmid (referred to as “SX-13bp-CCAAT”). This enabled transactivation by *NLRC5* (Figure 3A). Moreover, scrambling of the “CCAAT” sequence (referred to as “SX-13bp-CCTTT”) abrogated *NLRC5*-mediated transactivation, pinpointing the importance of this unique “Y” box (Figure 3A). *NLRC5* was also able to transactivate the

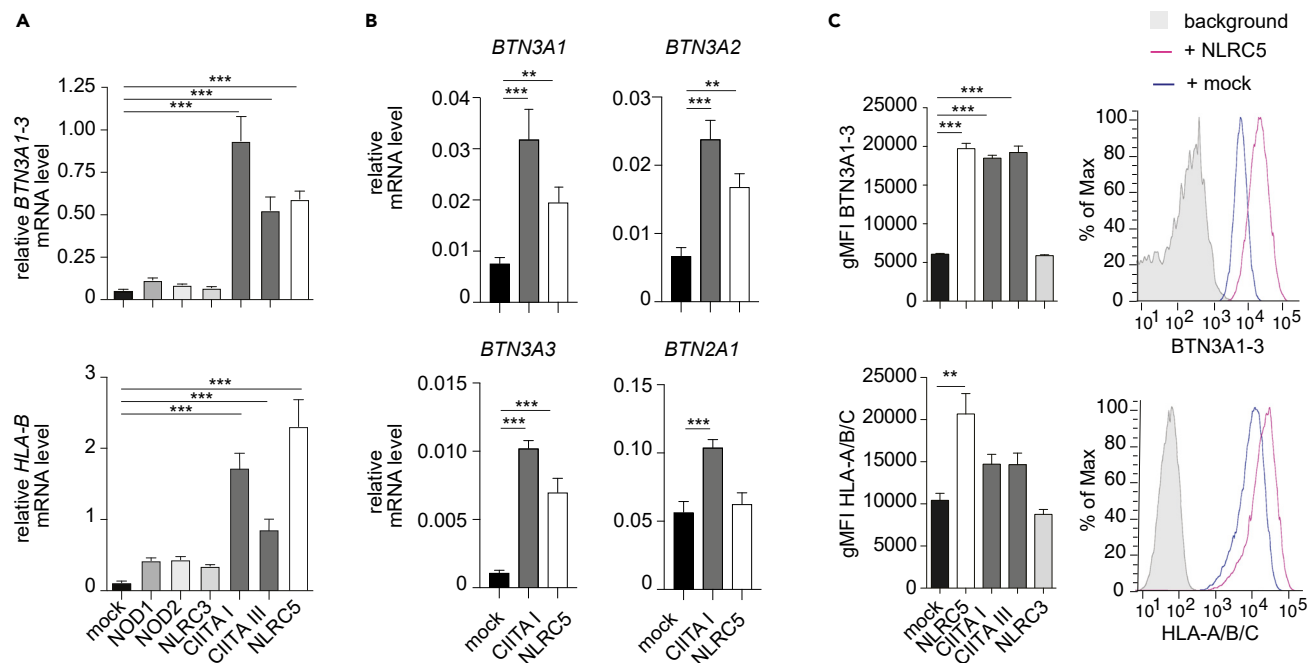


Figure 2. NLRC5 overexpression increases *BTN3A1-3* expression

(A and B) *BTN3A1-3*, *BTN2A1*, or *HLA-B* mRNA levels (relative to *POLR2A* mRNA) were measured by qRT-PCR 48 h following transfection of plasmids encoding the indicated NLR proteins or an empty vector (mock) in HEK293T.

(C) HEK293T cells were co-transfected with vectors coding for the indicated NLRs or empty vector (mock) and a GFP-encoding plasmid to identify transfected cells. Graphs depict the quantification of *HLA-A/B/C* and *BTN3A1-3* geometric MFI (gMFI) gating on GFP⁺ cells 48 h post-transfection. Histogram overlays show *HLA-A/B/C* and *BTN3A1-3* expression for background (gray), mock- (blue), and NLRC5-transfected (pink) HEK293T cells. (A–C) Results are depicted as mean \pm SD ($n = 3$ technical replicates) and are representative of at least two independent experiments. Statistical differences were determined by one-way ANOVA followed by comparison of the experimental conditions to the corresponding mock transfection and were corrected for multiple testing using the Dunnett method. Only statistically significant differences are illustrated. ** $p < 0.01$; *** $p < 0.001$.

“SX-13bp-CCAAT” *BTN3A1* promoter construct, which diverges from the “SX-13bp-CCAAT” *BTN3A2* reporter by only 2 bp in the S-box, in a CCAAT-dependent manner (Figure 3C). Not surprisingly, similar results were observed when overexpressing CIITA I (Figures 3D and 3E). These results reveal the presence of an unconventional SXY module in the *BTN3A* promoters.

The S-box and the distance of the CCAAT-box are key for NLRC5-mediated transactivation

One intriguing feature of the *BTN3A* promoters is the fact that the spacing between the X-box and the CCAAT sequence (13 bp) is shorter than the usual one found at the MHC promoters between the X-box and the ATTGG (usually 17–18 bp). To assess whether the unusual orientation and distance were important, we generated a luciferase reporter plasmid in which the CCAAT sequence of *BTN3A2* promoter was substituted by an ATTGG (referred to as “SX-13bp-ATTGG”) at the 13 bp distance from the X-box. Interestingly, this promoter was transactivated neither by NLRC5 nor by CIITA (Figure 4A). We also moved the CCAAT sequence 18 bp downstream of the X-box (referred to as “SX-18bp-CCAAT”). Again, NLRC5- and CIITA-mediated transactivation were impaired (Figure 4A). Yet, insertion of an ATTGG sequence at 18 bp distance from the X-box (referred to as “SX-18bp-ATTGG”), which mirrors the classical organization of the *HLA* promoters, restored transactivation by NLRC5 and CIITA (Figure 4A). These results show that both orientation and distance of the NFY-binding site are crucial for transcriptional induction by these NLRs.

As the S-box found in the promoters of the *BTN3A* genes exhibits similarity to the one required for NLRC5-mediated transactivation, we next assessed its contribution to the transactivation of the *BTN3A2* promoter. In line with results from the MHC class I gene promoter, scrambling the S-box sequence severely compromised NLRC5-mediated, but not CIITA-mediated, transactivation (Figure 4B). This underlines the importance of the S-box for NLRC5-mediated regulation.

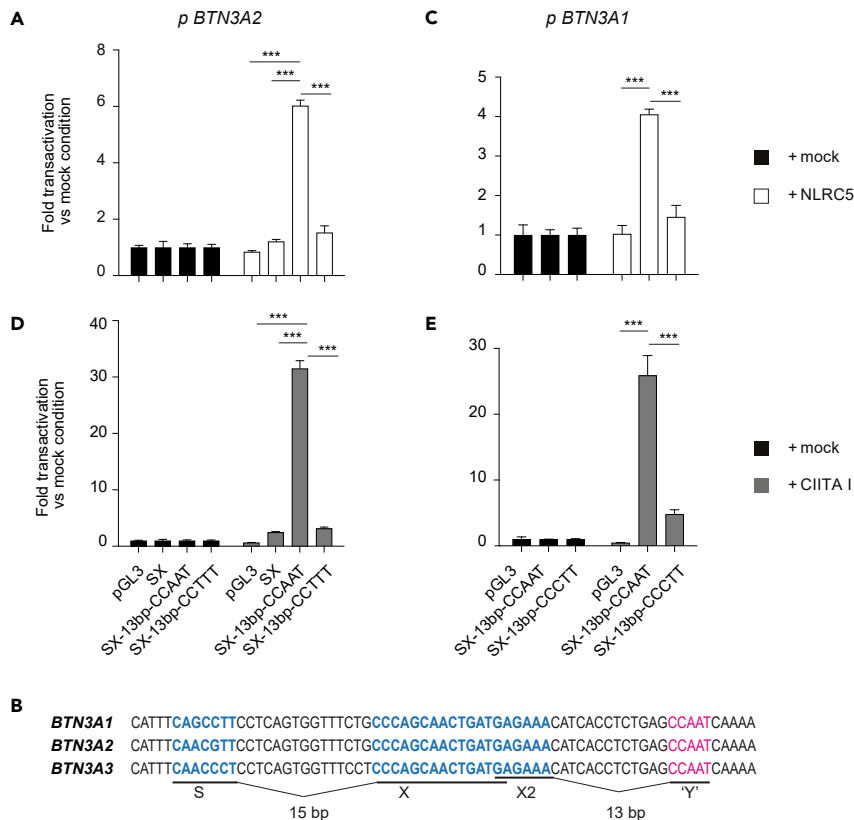


Figure 3. *BTN3A* genes harbor an atypical but functional SXY module

(A, C–E) Luciferase reporter assays were performed in HEK293T cells co-transfected with the parental pGL3 backbone or the indicated *BTN3A2* (A, D) or *BTN3A1* (C, E) promoter constructs, and an empty (mock) vector, or a vector coding for NLRC5 (A, C) or CIITA (D, E). SX-13bp-CCAAT contains the *BTN3A1* or *BTN3A2* promoter region, as indicated, with S-, X-, and 13 bp downstream CCAAT-box; where indicated, the CCAAT-box was mutated. (B) Alignment of the proximal *BTN3A1*-3 promoter region containing S- and X-motifs highlighted in blue and a 13 bp downstream “Y” CCAAT-box highlighted in pink. Distances between motifs are indicated. (A and C–E) Data are expressed as fold transactivation as compared with the mock condition. Results represent mean \pm SD of $n = 3$ (A and D) and $n = 4$ (C and E) technical replicates and are representative of at least two independent experiments. Statistical differences were determined by performing a two-way ANOVA followed by comparison of the SX-13bp-CCAAT condition to the others transfected with the same NLR and were corrected for multiple testing using the Holm-Sidak method. Only statistically significant differences are illustrated. *** $p < 0.001$.

BTN3A genes are direct targets of NLRC5

In order to prove that *BTN3A* genes are direct targets of NLRC5, we performed chromatin immunoprecipitation (ChIP) experiments. In the absence of an antibody against endogenous human NLRC5, we generated an HA-tagged version of wild-type NLRC5 (wt NLRC5) and of a mutant of the Walker A motif (mt NLRC5), which prevents NLRC5 nuclear translocation and transcriptional activity (Meissner et al., 2010). We then co-transfected HEK293T cells with plasmids coding for wt NLRC5 or mt NLRC5, and for the surface protein CD72, thus enabling the enrichment of transfected cells. ChIP using chromatin from wt NLRC5-transfected cells led to a substantial enrichment of the promoter region of *HLA-B* but also of *BTN3A1* and *BTN3A2* genes as compared with mt NLRC5-transfected cells (Figure 5). By contrast, the promoter of *HOXC8*, a gene not known to be controlled by NLRC5, was not enriched (Figure 5). Although we were unable to design primers specific for *BTN3A3* promoter due to the high homology of the regulatory regions of these genes, these data demonstrate occupation of *BTN3A1* and *A2* promoters by NLRC5 (Figure 5).

NLRC5 and *BTN3A* genes are co-regulated in health and disease

We next checked the correlation between *NLRC5* and *BTN3A1*-3 expression in human pathological conditions in which $\gamma\delta$ T cells are considered relevant. First, we analyzed transcriptomic data from a Gambia

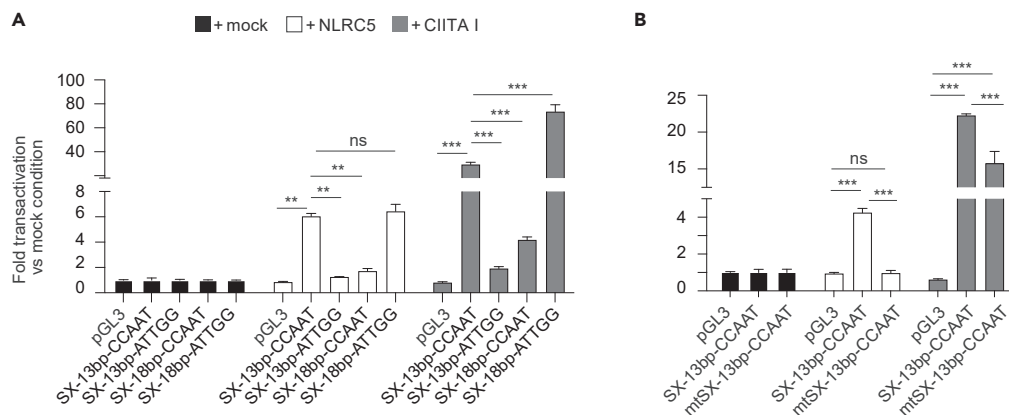


Figure 4. S-box sequence and CCAAT-box position are important for NLRC5 transactivation

(A and B) Luciferase reporter assays were performed in HEK293T cells co-transfected with the parental pGL3 backbone or the indicated *BTN3A2* promoter constructs, and a vector coding for NLRC5 or CIITA I, or an empty (mock) vector; mSX indicates a scrambled S-box sequence (the CAACGTT sequence was substituted by CCAGAGT) (B). Data are expressed as fold transactivation as compared to the mock condition. Results represent mean \pm SD of $n = 3$ technical replicates and are representative of at least three independent experiments. Statistical differences were determined by performing a two-way ANOVA followed by comparison of the indicated conditions and were corrected for multiple testing using the Holm-Sidak method. ** $p < 0.01$; *** $p < 0.001$; ns: not significant.

tuberculosis cohort study (Maertzdorf et al., 2011). A significant correlation of *NLRC5* with *BTN3A1* and *BTN3A2* expression was observed in healthy uninfected donors (Figure 6A). These correlations were stronger in donors latently infected with *M. tuberculosis* and in active tuberculosis (TB) patients (Figure 6A). For *BTN3A3*, a significant correlation with *NLRC5* was observed only in active TB patients (Figure 6A). Of note, the correlations of *BTN3A* genes with *CIITA* expression were lower, but still significant in most cases, whereas *BTN2A1* levels correlated with neither of the two NLRs (Figure S3A). Hierarchical clustering of the correlations for the entire cohort (i.e. all three groups) highlighted the close proximity of *NLRC5* to *BTN3A1*, *BTN3A2*, and *HLA-B*, whereas *BTN3A3* was more distant (Figure 6B). Corroborating the specificity of these results, *NECTIN2* and *PTPRC/CD45*, two genes not expected to be regulated by *NLRC5* or *CIITA*, were clustering at farther distances (Figure 6B). Taken together, these data highlight a potential role for *NLRC5* in anti-mycobacterial immunity.

We next investigated the correlation between *NLRC5* and *BTN3A1-3* mRNA levels across cancers in “The Cancer Genome Atlas” (TCGA; <https://www.cancer.gov/tcga>) provisional datasets. Given the very high expression of these genes in immune cells, we corrected for CD45 mRNA prior to sample analysis to reduce the confounding effect by infiltrating leukocytes (Figures 1C–1E) (Ludigs et al., 2016; Staehli et al., 2012). In most cancers, we found a significant correlation between *NLRC5* and *BTN3A1-3* transcript abundance (Figure 6C), whereas the correlation with *NECTIN2* was low and mostly non-significant (Figure S3B). The correlation with *HLA-B* was generally good, with the exception of the dlbc dataset (Figure S3B) (Yoshihama et al., 2016). We therefore tested an independent cohort of DLBCL samples (GSE10846; Figure S3C), which corroborated a generally weaker correlation between *NLRC5* and *HLA-B* than with the *BTN3A* genes. Across cancers, *BTN3A1-3* correlated better with *NLRC5* than with *CIITA* expression, whereas the profile of *BTN2A1* was quite independent from the transcript levels of both NLRs (Figure S3D).

We next investigated whether methylation of the *NLRC5* promoter inversely correlated with the expression of the *BTN3A* genes. Data supported this hypothesis, including for *HLA-B*, whereas barely significant and variable results were observed for *NECTIN2* (Figures 6D and S3E). We also interrogated whether structural alterations leading to *NLRC5* copy number loss were concomitant with *BTN3A* gene expression decrease. We thus focused on breast (brca) and prostate (prad) cancer, the only tumor sets having more than five samples lacking both *NLRC5* copies, and compared *BTN3A* expression of samples harboring loss of *NLRC5* (homozygous deletion, HDEL) with samples having normal copy number (WT). Despite the small sample size, *BTN3A1*, *BTN3A2*, as well as *HLA-B* gene expression were reduced in the absence of *NLRC5* (Figures 6E and S3F). As for most correlations tested in Figure 6, a similar trend was observed also for *BTN3A3*, although less robust (Figure 6E). We wondered whether the presence of a “C” instead of the conserved

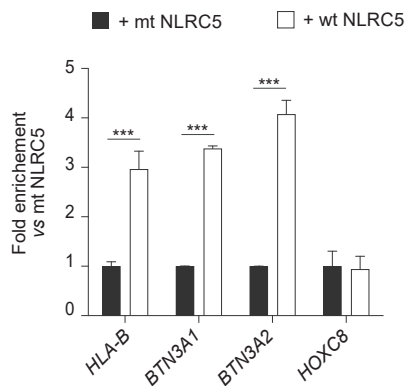


Figure 5. NLRC5 directly binds to *BTN3A* promoter regions

Vectors encoding human wild-type NLRC5 (wt NLRC5) or Walker A mutant (mt NLRC5) were cotransfected with CD72 into HEK293T. Forty-eight hours later, CD72-positive cells were MACS enriched and chromatin prepared. Binding of NLRC5 to the indicated promoters was assessed by chromatin immunoprecipitation (ChIP) followed by quantitative PCR. Results are expressed as fold enrichment as compared with the mt NLRC5 condition. Results are depicted as the mean \pm SD of $n = 3$ technical replicates and are representative of at least two independent experiments. Statistical differences were determined by performing a two-way ANOVA followed by comparison of the wt NLRC5 with mt NLRC5 transfection and were corrected for multiple testing using the Holm-Sidak method. *** $p < 0.001$.

“T” residue in the S-box of this gene’s promoter might underlie this observation (Figure S3G). We thus substituted this T with a C in the *BTN3A2* SX-13bp-CCAAT reporter plasmid. Supporting our hypothesis, this modification reduced NLRC5-mediated transactivation (Figure S3G). Taken together, these data underscore the robust correlation of NLRC5 with *BTN3A1* and *BTN3A2* transcript abundance in healthy and diseased conditions in which $V\gamma 9V\delta 2$ T cells are considered relevant.

NLRC5 overexpression confers susceptibility to $\gamma\delta$ T-cell-mediated killing

We thus overexpressed NLRC5 in Raji cells, a Burkitt lymphoma cell line known to trigger poor recognition by $V\gamma 9V\delta 2$ T cells (Harly et al., 2012). As our results predicted, polyclonal NLRC5-transduced Raji cells presented increased levels of *BTN3A1-3* surface expression as compared with mock-transduced control cells (Figure 7A). This was observed both in the absence and in the presence of zoledronate, a pharmacological inhibitor of the mevalonate pathway that increases IPP concentrations (Figure 7A). A similar trend was observed for HLA-A/B/C (Figure S4A). In a first set of experiments, killing of mock- or NLRC5-transduced polyclonal Raji cells was measured after 24 h of co-culture with *in-vitro*-expanded, primary $V\gamma 9V\delta 2$ T cells in the presence of zoledronate. NLRC5 overexpression significantly enhanced the specific killing of Raji cells (Figure 7B). In these experiments, polyclonal populations of target cells with a transduction efficiency of roughly 68% were used. As this could have masked the effect of NLRC5 overexpression on $V\gamma 9V\delta 2$ T-cell-mediated killing, we next generated subclones of mock- and NLRC5-transduced Raji cells. In line with data presented in Figure 2B, NLRC5-overexpressing subclones exhibited increased levels of *BTN3A1-3* transcripts, but no difference in *BTN2A1* mRNA (Figure 7C); in agreement, *BTN3A1-3* surface expression was augmented (Figure S4B). Co-culture of $V\gamma 9V\delta 2$ T cells with these subclones led to significantly increased IFN γ production (Figure S4C) and killing (Figure 7D). To demonstrate that this enhanced killing was mediated by the *BTN3A* molecules, we knocked out *BTN3A1* by CRISPR/Cas9 in the NLRC5-overexpressing subclone 2. This loss-of-function strategy led to a decrease in the transcript levels of *BTN3A1* and—due to the high homology of these two genes—of *BTN3A2* (Figure S4D). As expected, these cells exhibited significantly reduced susceptibility to be killed by $V\gamma 9V\delta 2$ T cells (Figure S4E). Therefore, NLRC5 overexpression not only increases the levels of *BTN3A1-3* but also functionally promotes $V\gamma 9V\delta 2$ T cell activation and killing.

DISCUSSION

The role of NLRC5 as a transcriptional regulator of MHC class I genes has been rapidly unveiled over the past years (Chelbi et al., 2017; Ludigs et al., 2015; Meissner et al., 2010, 2012a; Neerinx et al., 2012, 2013; Robbins et al., 2012; Staehli et al., 2012; Yao et al., 2012). Yet, our knowledge of its global transcriptional targets in humans remains limited. This work provides the first evidence for the transcriptional regulation of *BTN3A1-3* genes by NLRC5, broadening our understanding of its role in humans.

Analysis of promoter sequences of *BTN* genes that are clustered in the adjacent MHC locus highlighted the presence of SXY modules. One of these modules, in the *BTN2A2* promoter, is transactivated by CIITA (Sarter et al., 2016). In contrast, CIITA’s closest homolog NLRC5 did not contribute to the expression of *Btln2a2* in the tested immune organs, adding further evidence for the role of CIITA in regulating this gene. We also identified an SXY module in the promoter of *BTN2A1*, and our results indicate that its expression is largely dependent on the RFX complex. However, *BTN2A1* transcript levels, which were not increased by NLRC5

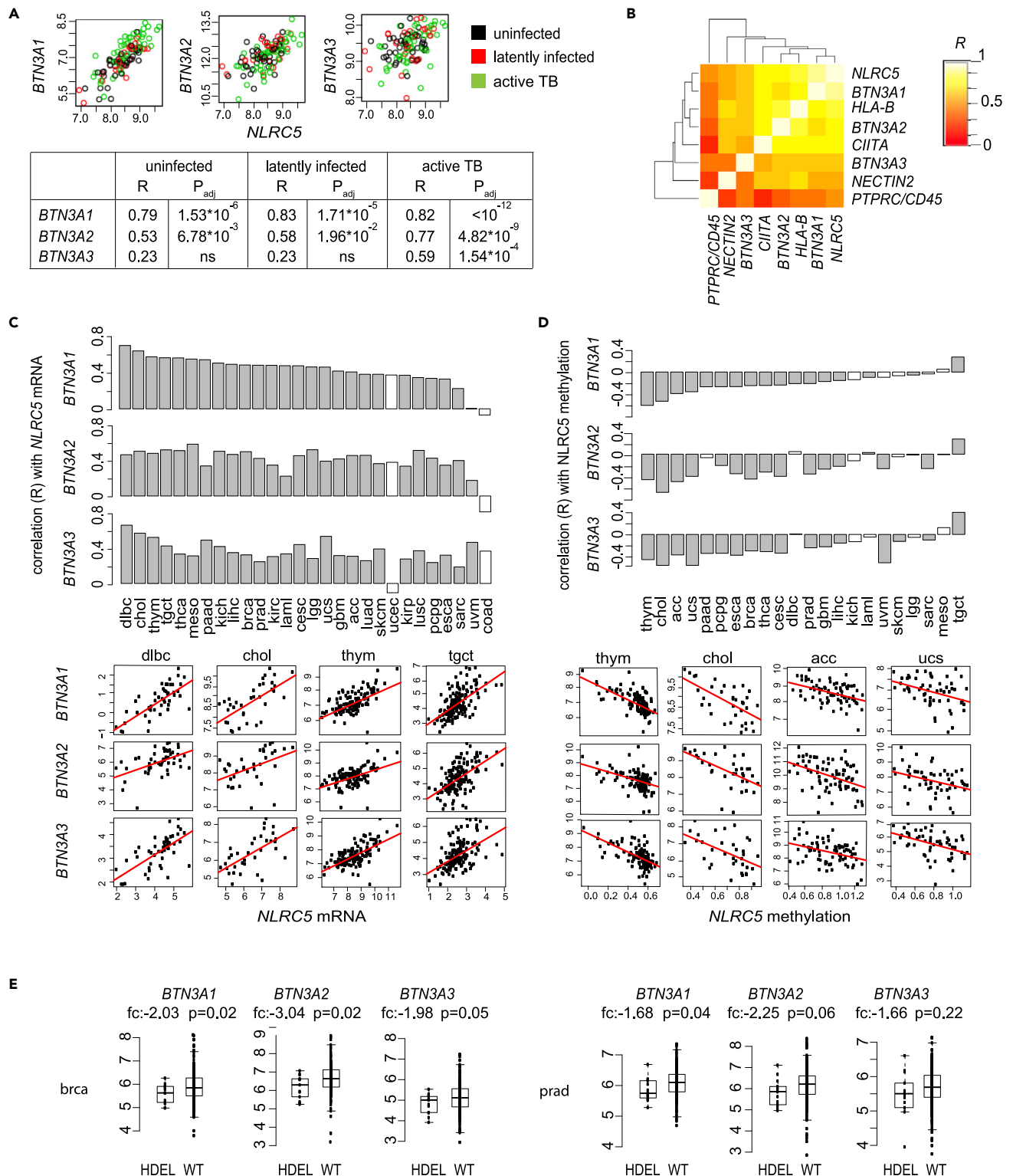


Figure 6. *BTN3A1-3* expression correlates with *NLRC5* levels

(A and B) Pairwise correlation of *NLRC5* and *BTN3A1*, *BTN3A2*, *BTN3A3* expression are visualized. Analyses were performed using transcriptome datasets of the Gambia *M. tuberculosis* (TB) cohort study (GSE28623). (A) Scatterplots of gene expression are shown. The samples are divided in the groups “uninfected” (black), “latently infected” (red), and “active TB” (green). The table displays the Spearman’s correlation coefficient (R), and Bonferroni adjusted

Figure 6. Continued

p values (p, adj) for the 3 groups. (B) Pairwise correlations of *NLRC5* and selected genes are visualized using a heatmap and hierarchical clustering tree of Spearman's rank correlations. Correlations were calculated on the entire cohort.

(C–E) Data from The Cancer Genome Atlas (TCGA) provisional dataset collections were analyzed after adjustment for *CD45* expression. (C) Spearman's correlation coefficient (R values) for *NLRC5* and *BTN3A1*, *BTN3A2*, or *BTN3A3* mRNA expression across cancer types. Scatterplots are shown for the top-ranked cancer types. (D) Spearman's correlation coefficient for *NLRC5* promoter methylation and *BTN3A1*, *BTN3A2*, or *BTN3A3* mRNA expression across cancer types. Scatterplots are shown for the best-ranked cancer types. (C, D) Gray bars indicate significant correlations ($p < 0.05$ after Bonferroni correction) and white bars non-significant ones. (E) *BTN3A1*, *BTN3A2*, and *BTN3A3* mRNA abundance is plotted according to *NLRC5* copy number status. fc: fold change of expression in HDEL ($n = 14$ and $n = 13$ for brca and prad, respectively) over WT group ($n = 272$ and $n = 361$ for brca and prad, respectively). HDEL: homozygous deletion; WT: wild type. Two group comparisons were performed using unpaired t tests, two-tailed, unequal variance, and p values are indicated. Cancer types' abbreviations are described in the [Transparent Methods](#) section.

and moderately by *CIITA*, poorly correlated with these NLRs. Additional analyses are therefore needed to understand the transcriptional regulation of this gene. Further, data from BLS-derived B cell lines indicate that the induction of the *BTN3A* genes is also largely dependent on the presence of an enhanceosome, raising new questions on $\gamma\delta$ T cell subsets in BLS patients.

Here, we identified an atypical SXY module in the promoters of *BTN3A1-3* genes. Classical, non-classical, and selected MHC-related gene promoters contain—next to the S- and X-motif—an ATTGG Y-box (Krawczyk et al., 2008; Ludigs et al., 2015). Instead, the module of *BTN3A1-3* promoters corresponds to the consensus sequence occupied by *NLRC5* with regard to the S- and X-boxes but contains the reverse complement of the Y-box. This “CCAAT” sequence corresponds to the canonical regulatory motif occupied by the trimeric NFY complex (Dolfini et al., 2012). Interestingly, the promoter of the MHC-class II-associated invariant chain (Ii, also called CD74) also contains an atypical SXY, with the CCAAT motif at a reduced distance from the X-box (Brown et al., 1991; Doyle et al., 1990; Zhu and Jones, 1990). This is in line with our observations in the *BTN3A* promoter, in which both orientation and spacing of the Y-box are crucial for *NLRC5*-mediated transactivation, presumably through formation of an alternative enhanceosome complex. Finally, we substantiate the importance of the S-box by showing that the substitution of a single conserved position affects *NLRC5*-mediated transactivation, possibly contributing to differences in the expression of individual *BTN3A* genes.

Importantly, overexpressed, but not endogenous, *CIITA* transactivates MHC class I genes, questioning its physiological contribution to *BTN3A1-3* gene transcription (Chang et al., 1996; Gobin et al., 1997; Ludigs et al., 2015; Martin et al., 1997; Robbins et al., 2012; Williams et al., 1998). This is corroborated by the observation that *CIITA* deficiency did not reduce *BTN3A* expression in B cell lines. Although the question on the physiological contribution to *BTN3A1-3* transcription is open also for *NLRC5*, robust correlative data support this possibility. *BTN3A1-3* expression is abundant in T and NK cells, similar to the profile of *NLRC5* (Neerinx et al., 2010; Staehli et al., 2012; Wu et al., 2009). The S-box in *BTN3A1-3* promoters strongly resembles the one of *NLRC5*-transactivated genes (Ludigs et al., 2015; Meissner et al., 2012b). In the blood of both uninfected and *M. tuberculosis*-infected individuals, expression of *NLRC5* strongly correlated with the one of *BTN3A1*, which stimulates PAg-mediated activation of $V\gamma 9V\delta 2$ T cells (Harly et al., 2012). Finally, we observed a robust coregulation between *BTN3A1/BTN3A2* and *NLRC5* expression in various cancers, and *NLRC5* homozygous deletion was associated with a decrease in the abundance of *BTN3A1* and *BTN3A2* mRNA (Maertzdorf et al., 2011). Therefore, although we do not exclude a contribution of *CIITA* or a redundant function by these NLRs in the regulation of these genes, our results support a role for *NLRC5* in regulating *BTN3A* gene transcription in normal as well as pathological conditions such as TB or cancer.

Our data demonstrate that forcing the expression of *NLRC5* in cancerous target cells significantly promotes their killing by $V\gamma 9V\delta 2$ T cells, highlighting a novel functional link between *NLRC5* expression and cytotoxicity by unconventional T cells. Because *NLRC5* overexpression did not significantly impact *BTN2A1* expression, and MHC I and B2M are known to be dispensable and even hinder the activation of these unconventional T cells by engaging surface inhibitory receptors typical of NK cells (Bakker et al., 1998; Carena et al., 1997; Fisch et al., 1997; Halary et al., 1997; Morita et al., 1995), *BTN3A* molecules constitute the best candidates responsible for the *NLRC5*-driven enhanced $V\gamma 9V\delta 2$ T-cells-mediated killing. In accordance, CRISPR-mediated knockdown of *BTN3A* molecules nearly abrogated the killing enhancement induced by *NLRC5* overexpressing cells. *NLRC5* has already been linked to antitumor responses and patient prognosis (Farashi et al., 2019; Fernandez-Jimenez et al., 2019; Wang et al., 2019; Yoshihama et al., 2016). Although this has been attributed to its regulation of the MHC class I pathway, it will be important to

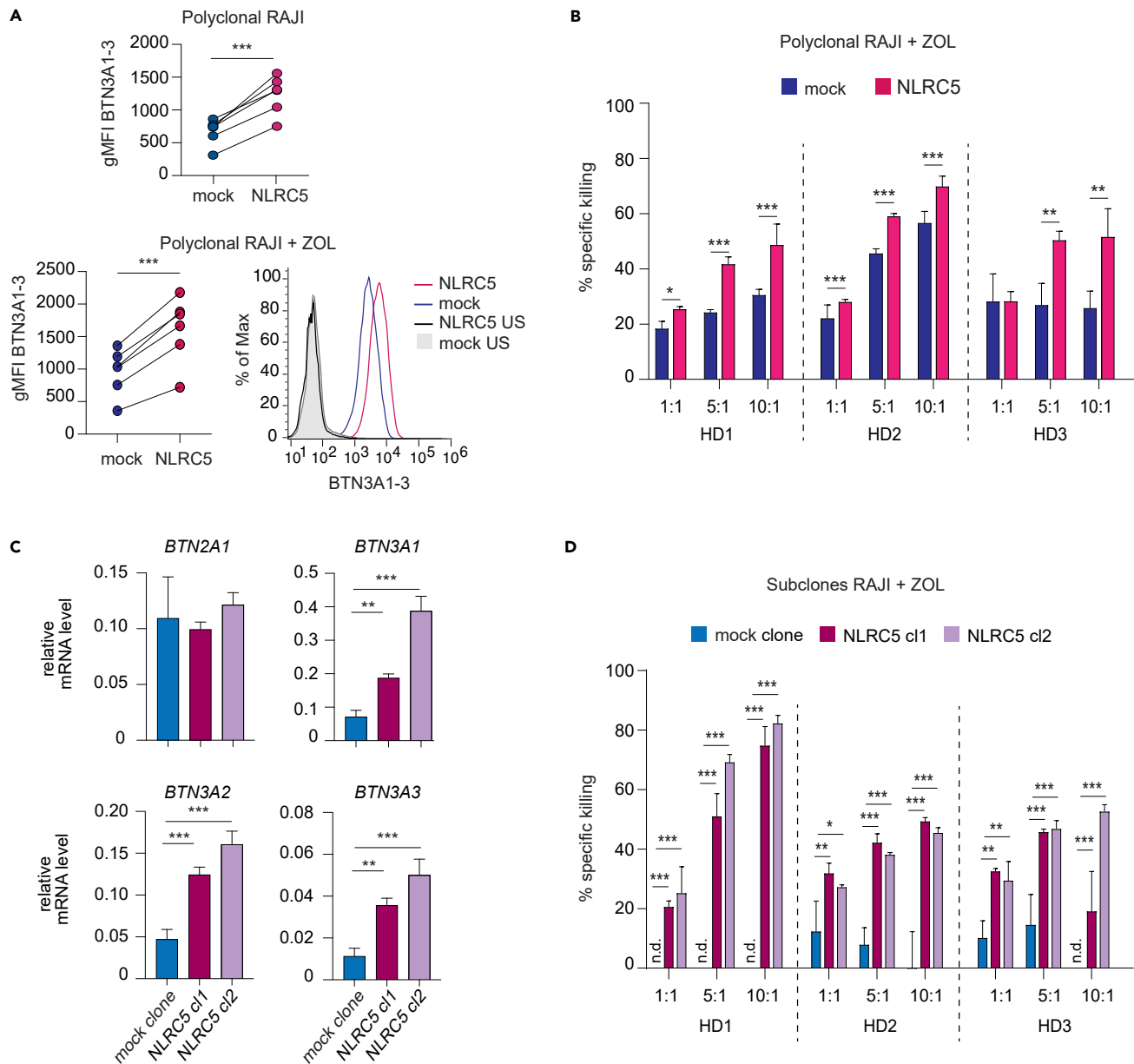


Figure 7. NLRC5 favors the activation of V γ 9V δ 2 T cells

(A) Polyclonal Raji cells were transduced with NLRC5-coding or mock vector and treated with zoledronate (+ZOL) for 24 h (bottom panel) or left untreated (top panel). BTN3A1-3 surface expression was analyzed by flow cytometry. Graphs depict a quantification of BTN3A1-3 geometric MFI (gMFI; top and bottom left), and the histogram overlays (bottom right) show BTN3A1-3 expression for unstained (US; black, gray), mock- (blue) and NLRC5-transfected polyclonal Raji cells (pink). Results represent six independent measurements.

(B) Specific killing of NLRC5- (pink) or mock-transduced polyclonal Raji cells (blue) was measured after 24 h of co-culture with V γ 9V δ 2 T cells at 3 effector-to-target ratios (1:1, 5:1, and 10:1) in the presence of ZOL. Depicted are the results for three independent healthy donors (HD) as mean \pm SD (n = 3 technical replicates). The results are representative of four independent healthy donors and three independent experiments.

(C) *BTN2A1* and *BTN3A1*, A2, and A3 mRNA levels (relative to *POLR2A* mRNA) were assessed by qRT-PCR in the NLRC5- (red and violet) or mock-transduced Raji subclones (blue). The results depict mean \pm SD (n = 3 technical replicates) and are representative of 2 independent experiments.

(D) Specific killing of the NLRC5- or mock-transduced Raji subclones was measured after 24 h of co-culture with V γ 9V δ 2 T cells at 3 effector-to-target ratios in the presence of ZOL. n.d. correspond to conditions where no specific lysis of the target cells by the V γ 9V δ 2 T cells was detected. Depicted are the results for three independent healthy donors (HD) as mean \pm SD (n = 3 technical replicates). The results are representative of six independent healthy donors and three independent experiments. (A–D) Statistical differences between the condition with and without NLRC5 overexpression were calculated using paired Student's t test (A) or post hoc Student's tests adjusted for multiple comparisons using the Holm-Sidak method (B–D). *p \leq 0.05, **p \leq 0.01, ***p \leq 0.001.

Only statistically significant differences are illustrated.

consider the potential contribution of the hereby discovered NLRC5/BTN3A regulation axis because altered expression of *BTN3A* genes has been associated with cancer and other diseases (Benyamine et al., 2017; Blazquez et al., 2018; Le Page et al., 2012; Peedicayil et al., 2010; Viken et al., 2009). Indeed, intratumoral $\gamma\delta$ T cells have emerged as the most significant favorable cancer-wide prognostic infiltrating immune subset, and $\gamma\delta$ T-cell-based clinical trials are increasingly performed, expanding our portfolio of immunotherapeutical approaches (Gentles et al., 2015). In addition to its role in the activation of $\gamma\delta$ T cells, recent findings illustrate how *BTN3A1* can play an inhibitory function on $\alpha\beta$ T cells, by hindering the segregation of the phosphatase CD45 from the immune synapse (Payne et al., 2020). Importantly, this inhibition is relieved upon zoledronate treatment or by the use of CD277-specific agonistic antibodies, which enable the concomitant activation of $V\gamma9V\delta2$ T cells. Our discoveries indicate therefore that targeting the NLRC5 axis, possibly in combination with such treatments, might represent an attractive anti-cancer strategy leveraging on both $\alpha\beta$ and $\gamma\delta$ T cells.

Our results suggest that, in humans, NLRC5 regulates more genes than previously thought and challenge its role as a transactivator of MHC class I and related genes only (Ludigs et al., 2015). *BTN3A1* molecules have recently been shown to mediate $V\gamma9V\delta2$ T cell activation in response to host- or microbial-derived metabolites, suggesting an involvement of NLRC5 in the $\gamma\delta$ T-cell-mediated host immunity (Benyamine et al., 2016; Harly et al., 2012; Sandstrom et al., 2014; Vavassori et al., 2013). This observation is in agreement with previous findings that NLRC5 regulates non-classical MHC class I genes, such as murine H2-T10/H2-T22, which are recognized by a fraction of $\gamma\delta$ T cells (Crowley et al., 2000). Therefore, regulation of *BTN3A1* transcription by NLRC5 shows strong parallels with its established function, reinforcing its role as a modulator of conventional and unconventional T cell immunity.

Limitations of the study

Even if *BTN3A* molecules are induced by NLRC5 and required for $V\gamma9V\delta2$ T cell activation, we cannot rule out the possibility that other NLRC5 targets, known or unknown, might contribute to the observed effect. In addition, further experiments are required to prove the pathophysiological relevance of these findings in cancer or infection.

Resource availability

Lead contact

Requests for further information and reagents should be directed to and will be fulfilled by the Lead Contact Greta Guarda (greta.guarda@irb.usi.ch).

Materials availability

Materials generated in this study will be made available upon reasonable request and may require a material transfer agreement.

Data and code availability

This study did not generate datasets or analyze codes.

METHODS

All methods can be found in the accompanying [Transparent Methods supplemental file](#).

SUPPLEMENTAL INFORMATION

Supplemental Information can be found online at <https://doi.org/10.1016/j.isci.2020.101900>.

ACKNOWLEDGMENTS

We thank S. Monticelli (IRB, Bellinzona) for critical reading of the manuscript and help. We thank R. Spaapen (Sanquin Research, Amsterdam), P. Van den Elsen (Leiden University, Leiden), M. Kornete and L. Jeker (University of Basel, Basel), R. Mantovani (Università degli Studi di Milano, Milan), F. Bertoni (IOR, Bellinzona), T. Kufer (University of Hohenheim, Hohenheim), D. Cohen and K. Ludigs (during their time at the University of Lausanne (UNIL), Lausanne), and M. Juilland and M. Thome (UNIL, Lausanne) for reagents and/or technical help. We thank the UNIL for sharing transgenic mice. This work was supported by the Swiss National Science Foundation [PP00P3_139094, PP00P3_165833, and 310030_185185].

to G.G.), the European Research Council [ERC-2012-StG310890 to G.G.], and the Fondazione San Salvatore, Lugano. This work was partially supported by the German Research Foundation (DFG) [EXC-294 (BIOS), EXC-2189 (CIBSS) and SFB850 (C10) to S.M.].

AUTHOR CONTRIBUTIONS

A.T.D., J.S., A.Z., H.J.K., S.M.B., G.C., and S.T.C. performed the experiments; L.L., S.T.C., P.V.E., S.K., W.R., and S.M. shared reagents, help, and advice; I. K. performed the bioinformatic analyses; A.T.D., J.S., I.K., S.T.C., S.M., and G.G. designed the research, analyzed the data, and wrote the manuscript.

DECLARATION OF INTERESTS

Other projects in G.G. laboratory are supported by OM-Pharma, Meyrin, IFM Therapeutics, Boston, and Novartis Foundation. Unrelated projects in SM laboratory are supported by the Eurostars program (EUROPEAN UNION HORIZON, 2020 FRAMEWORK PROGRAM).

Received: March 20, 2020

Revised: November 23, 2020

Accepted: December 1, 2020

Published: January 22, 2021

REFERENCES

- Abeler-Dorner, L., Swamy, M., Williams, G., Hayday, A.C., and Bas, A. (2012). Butyrophilins: an emerging family of immune regulators. *Trends Immunol.* 33, 34–41.
- Anderson, D.A., 3rd, Grajales-Reyes, G.E., Satpathy, A.T., Vasquez Hueichucura, C.E., Murphy, T.L., and Murphy, K.M. (2017). Revisiting the specificity of the MHC class II transactivator CIITA in classical murine dendritic cells in vivo. *Eur. J. Immunol.* 47, 1317–1323.
- Arnett, H.A., and Viney, J.L. (2014). Immune modulation by butyrophilins. *Nat. Rev. Immunol.* 14, 559–569.
- Bakker, A.B., Phillips, J.H., Figdor, C.G., and Lanier, L.L. (1998). Killer cell inhibitory receptors for MHC class I molecules regulate lysis of melanoma cells mediated by NK cells, gamma delta T cells, and antigen-specific CTL. *J. Immunol.* 160, 5239–5245.
- Benyamine, A., Le Roy, A., Mamessier, E., Gertner-Dardenne, J., Castanier, C., Orlanducci, F., Pouyet, L., Goubard, A., Collette, Y., Vey, N., et al. (2016). BTN3A molecules considerably improve Vgamma9Vdelta2 T cells-based immunotherapy in acute myeloid leukemia. *Oncoimmunology* 5, e1146843.
- Benyamine, A., Loncle, C., Foucher, E., Blazquez, J.L., Castanier, C., Chretien, A.S., Modesti, M., Secq, V., Chouaib, S., Gironella, M., et al. (2017). BTN3A is a prognosis marker and a promising target for Vgamma9Vdelta2 T cells based-immunotherapy in pancreatic ductal adenocarcinoma (PDAC). *Oncoimmunology* 7, e1372080.
- Blazquez, J.L., Benyamine, A., Pasero, C., and Olive, D. (2018). New insights into the regulation of gammadelta T cells by BTN3A and other BTN/ BTNL in tumor immunity. *Front. Immunol.* 9, 1601.
- Brown, A.M., Barr, C.L., and Ting, J.P. (1991). Sequences homologous to class II MHC W, X, and Y elements mediate constitutive and IFN-gamma-induced expression of human class II-associated invariant chain gene. *J. Immunol.* 146, 3183–3189.
- Carena, I., Shamsiev, A., Donda, A., Colonna, M., and Libero, G.D. (1997). Major histocompatibility complex class I molecules modulate activation threshold and early signaling of T cell antigen receptor-gamma/delta stimulated by nonpeptidic ligands. *J. Exp. Med.* 186, 1769–1774.
- Chang, C.H., Guerder, S., Hong, S.C., van Ewijk, W., and Flavell, R.A. (1996). Mice lacking the MHC class II transactivator (CIITA) show tissue-specific impairment of MHC class II expression. *Immunity* 4, 167–178.
- Chelbi, S.T., Dang, A.T., and Guarda, G. (2017). Emerging major histocompatibility complex class I-related functions of NLR5. *Adv. Immunol.* 133, 89–119.
- Cheng, C., Wang, B., Gao, L., Liu, J., Chen, X., Huang, H., and Zhao, Z. (2018). Next generation sequencing reveals changes of the gammadelta T cell receptor repertoires in patients with pulmonary tuberculosis. *Sci. Rep.* 8, 3956.
- Crowley, M.P., Fahrer, A.M., Baumgarth, N., Hampl, J., Gutgemann, I., Teyton, L., and Chien, Y. (2000). A population of murine gammadelta T cells that recognize an inducible MHC class IIb molecule. *Science* 287, 314–316.
- De Libero, G., Lau, S.Y., and Mori, L. (2014). Phosphoantigen presentation to TCR gammadelta cells, a conundrum getting less gray zones. *Front. Immunol.* 5, 679.
- Dolfini, D., Gatta, R., and Mantovani, R. (2012). NF- κ B and the transcriptional activation of CCAAT promoters. *Crit. Rev. Biochem. Mol. Biol.* 47, 29–49.
- Doyle, C., Ford, P.J., Ponath, P.D., Spies, T., and Strominger, J.L. (1990). Regulation of the class II-associated invariant chain gene in normal and mutant B lymphocytes. *Proc. Natl. Acad. Sci. U S A* 87, 4590–4594.
- Farashi, S., Kryza, T., Clements, J., and Batra, J. (2019). Post-GWAS in prostate cancer: from genetic association to biological contribution. *Nat. Rev. Cancer* 19, 46–59.
- Fernandez-Jimenez, N., Garcia-Etxebarria, K., Plaza-Izurrieta, L., Romero-Garmendia, I., Jauregi-Miguel, A., Legarda, M., Ecsedi, S., Castellanos-Rubio, A., Cahais, V., Cuenin, C., et al. (2019). The methylome of the celiac intestinal epithelium harbours genotype-independent alterations in the HLA region. *Sci. Rep.* 9, 1298.
- Fisch, P., Meuer, E., Pende, D., Rothenfusser, S., Viale, O., Kock, S., Ferrone, S., Fradelizi, D., Klein, G., Moretta, L., et al. (1997). Control of B cell lymphoma recognition via natural killer inhibitory receptors implies a role for human Vgamma9/Vdelta2 T cells in tumor immunity. *Eur. J. Immunol.* 27, 3368–3379.
- Gentles, A.J., Newman, A.M., Liu, C.L., Bratman, S.V., Feng, W., Kim, D., Nair, V.S., Xu, Y., Khuong, A., Hoang, C.D., et al. (2015). The prognostic landscape of genes and infiltrating immune cells across human cancers. *Nat. Med.* 21, 938–945.
- Gobin, S.J., Peijnenburg, A., Keijsers, V., and van den Elsen, P.J. (1997). Site alpha is crucial for two routes of IFN gamma-induced MHC class I transactivation: the ISRE-mediated route and a novel pathway involving CIITA. *Immunity* 6, 601–611.
- Gu, S., Sachleben, J.R., Boughter, C.T., Nawrocka, W.I., Borowska, M.T., Tarrasch, J.T., Skiniotis, G., Roux, B., and Adams, E.J. (2017). Phosphoantigen-induced conformational change of butyrophilin 3A1 (BTN3A1) and its implication on Vgamma9Vdelta2 T cell activation. *Proc. Natl. Acad. Sci. U S A* 114, E7311–E7320.
- Halary, F., Peyrat, M.A., Champagne, E., Lopez-Botet, M., Moretta, A., Moretta, L., Vie, H., Fournie, J.J., and Bonneville, M. (1997). Control of self-reactive cytotoxic T lymphocytes expressing gamma delta T cell receptors by natural killer inhibitory receptors. *Eur. J. Immunol.* 27, 2812–2821.

- Harly, C., Guillaume, Y., Nedellec, S., Peigne, C.M., Monkkonen, H., Monkkonen, J., Li, J., Kuball, J., Adams, E.J., Netzer, S., et al. (2012). Key implication of CD277/butyrophilin-3 (BTN3A) in cellular stress sensing by a major human gammadelta T-cell subset. *Blood* **120**, 2269–2279.
- Jongsma, M.L.M., Guarda, G., and Spaapen, R.M. (2019). The regulatory network behind MHC class I expression. *Mol. Immunol.* **113**, 16–21.
- Kabelitz, D., Bender, A., Prospero, T., Wesselborg, S., Janssen, O., and Pechhold, K. (1991). The primary response of human gamma/delta + T cells to *Mycobacterium tuberculosis* is restricted to V gamma 9-bearing cells. *J. Exp. Med.* **173**, 1331–1338.
- Karunakaran, M.M., Willcox, C.R., Salim, M., Paletta, D., Fichtner, A.S., Noll, A., Starick, L., Nohren, A., Begley, C.R., Berwick, K.A., et al. (2020). Butyrophilin-2A1 directly binds germline-encoded regions of the *Vgamma9Vdelta2* TCR and is essential for phosphoantigen sensing. *Immunity* **52**, 487–498 e486.
- Krawczyk, M., Peyraud, N., Rybtsova, N., Masternak, K., Bucher, P., Barras, E., and Reith, W. (2004). Long distance control of MHC class II expression by multiple distal enhancers regulated by regulatory factor X complex and CIITA. *J. Immunol.* **173**, 6200–6210.
- Krawczyk, M., Seguin-Estevez, Q., Leimgruber, E., Sperisen, P., Schmid, C., Bucher, P., and Reith, W. (2008). Identification of CIITA regulated genetic module dedicated for antigen presentation. *PLoS Genet.* **4**, e1000058.
- Le Page, C., Marineau, A., Bonza, P.K., Rahimi, K., Cyr, L., Labouba, I., Madore, J., Delvoe, N., Mes-Masson, A.M., Provencher, D.M., et al. (2012). *BTN3A2* expression in epithelial ovarian cancer is associated with higher tumor infiltrating T cells and a better prognosis. *PLoS one* **7**, e38541.
- Ludigs, K., Jandus, C., Utschneider, D.T., Staehli, F., Bessoles, S., Dang, A.T., Rota, G., Castro, W., Zehn, D., Vivier, E., et al. (2016). *NLR5* shields T lymphocytes from NK-cell-mediated elimination under inflammatory conditions. *Nat. Commun.* **7**, 10554.
- Ludigs, K., Seguin-Estevez, Q., Lemeille, S., Ferrero, I., Rota, G., Chelbi, S., Mattmann, C., MacDonald, H.R., Reith, W., and Guarda, G. (2015). *NLR5* exclusively transactivates MHC class I and related genes through a distinctive *SXY* module. *PLoS Genet.* **11**, e1005088.
- Maertzdorf, J., Ota, M., Reipsilber, D., Mollenkopf, H.J., Weiner, J., Hill, P.C., and Kaufmann, S.H. (2011). Functional correlations of pathogenesis-driven gene expression signatures in tuberculosis. *PLoS one* **6**, e26938.
- Martin, B.K., Chin, K.C., Olsen, J.C., Skinner, C.A., Dey, A., Ozato, K., and Ting, J.P. (1997). Induction of MHC class I expression by the MHC class II transactivator CIITA. *Immunity* **6**, 591–600.
- Masternak, K., Peyraud, N., Krawczyk, M., Barras, E., and Reith, W. (2003). Chromatin remodeling and extragenic transcription at the MHC class II locus control region. *Nat. Immunol.* **4**, 132–137.
- Meissner, T.B., Li, A., Biswas, A., Lee, K.H., Liu, Y.J., Bayir, E., Iliopoulos, D., van den Elsen, P.J., and Kobayashi, K.S. (2010). NLR family member *NLR5* is a transcriptional regulator of MHC class I genes. *Proc. Natl. Acad. Sci. U S A* **107**, 13794–13799.
- Meissner, T.B., Li, A., and Kobayashi, K.S. (2012a). *NLR5*: a newly discovered MHC class I transactivator (CITA). *Microbes Infect.* **14**, 477–484.
- Meissner, T.B., Liu, Y.J., Lee, K.H., Li, A., Biswas, A., van Eggermond, M.C., van den Elsen, P.J., and Kobayashi, K.S. (2012b). *NLR5* cooperates with the RFX transcription factor complex to induce MHC class I gene expression. *J. Immunol.* **188**, 4951–4958.
- Morita, C.T., Beckman, E.M., Bukowski, J.F., Tanaka, Y., Band, H., Bloom, B.R., Golan, D.E., and Brenner, M.B. (1995). Direct presentation of nonpeptide prenyl pyrophosphate antigens to human gamma delta T cells. *Immunity* **3**, 495–507.
- Neerinx, A., Castro, W., Guarda, G., and Kufer, T.A. (2013). *NLR5*, at the heart of antigen presentation. *Front. Immunol.* **4**, 397.
- Neerinx, A., Lautz, K., Menning, M., Kremmer, E., Zigrino, P., Hosel, M., Buning, H., Schwarzenbacher, R., and Kufer, T.A. (2010). A role for the human nucleotide-binding domain, leucine-rich repeat-containing family member *NLR5* in antiviral responses. *J. Biol. Chem.* **285**, 26223–26232.
- Neerinx, A., Rodriguez, G.M., Steimle, V., and Kufer, T.A. (2012). *NLR5* controls basal MHC class I gene expression in an MHC enhancosome-dependent manner. *J. Immunol.* **188**, 4940–4950.
- Payne, K.K., Mine, J.A., Biswas, S., Chaurio, R.A., Perales-Puchalt, A., Anadon, C.M., Costich, T.L., Harro, C.M., Walrath, J., Ming, Q., et al. (2020). *BTN3A1* governs antitumor responses by coordinating alphabeta and gammadelta T cells. *Science* **369**, 942–949.
- Peedicayil, A., Vierkant, R.A., Hartmann, L.C., Fridley, B.L., Fredericksen, Z.S., White, K.L., Elliott, E.A., Phelan, C.M., Tsai, Y.Y., Berchuck, A., et al. (2010). Risk of ovarian cancer and inherited variants in relapse-associated genes. *PLoS one* **5**, e8884.
- Reith, W., and Mach, B. (2001). The bare lymphocyte syndrome and the regulation of MHC expression. *Annu. Rev. Immunol.* **19**, 331–373.
- Riano, F., Karunakaran, M.M., Starick, L., Li, J., Scholz, C.J., Kunzmann, V., Olive, D., Amslinger, S., and Herrmann, T. (2014). *Vgamma9Vdelta2* TCR-activation by phosphorylated antigens requires butyrophilin 3 A1 (*BTN3A1*) and additional genes on human chromosome 6. *Eur. J. Immunol.* **44**, 2571–2576.
- Rigau, M., Ostrouska, S., Fulford, T.S., Johnson, D.N., Woods, K., Ruan, Z., McWilliam, H.E.G., Hudson, C., Tutuka, C., Wheatley, A.K., et al. (2020). Butyrophilin 2A1 is essential for phosphoantigen reactivity by gammadelta T cells. *Science* **367**, eaay5516.
- Robbins, G.R., Truax, A.D., Davis, B.K., Zhang, L., Brickey, W.J., and Ting, J.P. (2012). Regulation of class I major histocompatibility complex (MHC) by nucleotide-binding domain, leucine-rich repeat-containing (NLR) proteins. *J. Biol. Chem.* **287**, 24294–24303.
- Sandstrom, A., Peigne, C.M., Leger, A., Crooks, J.E., Konczak, F., Gesnel, M.C., Breathnach, R., Bonneville, M., Scotet, E., and Adams, E.J. (2014). The intracellular B30.2 domain of butyrophilin 3A1 binds phosphoantigens to mediate activation of human *Vgamma9Vdelta2* T cells. *Immunity* **40**, 490–500.
- Sarter, K., Leimgruber, E., Gobet, F., Agrawal, V., Dunand-Sauthier, I., Barras, E., Mastelic-Gavillet, B., Kamath, A., Fontannaz, P., Guery, L., et al. (2016). *Btn2a2*, a T cell immunomodulatory molecule coregulated with MHC class II genes. *J. Exp. Med.* **213**, 177–187.
- Smith, I.A., Knezevic, B.R., Ammann, J.U., Rhodes, D.A., Aw, D., Palmer, D.B., Mather, I.H., and Trowsdale, J. (2010). *BTN1A1*, the mammary gland butyrophilin, and *BTN2A2* are both inhibitors of T cell activation. *J. Immunol.* **184**, 3514–3525.
- Staehli, F., Ludigs, K., Heinz, L.X., Seguin-Estevez, Q., Ferrero, I., Braun, M., Schroder, K., Rebsamen, M., Tardivel, A., Mattmann, C., et al. (2012). *NLR5* deficiency selectively impairs MHC class I-dependent lymphocyte killing by cytotoxic T cells. *J. Immunol.* **188**, 3820–3828.
- Tarantelli, C., Gaudio, E., Arribas, A.J., Kwee, I., Hillmann, P., Rinaldi, A., Cascione, L., Spriano, F., Bernasconi, E., Guidetti, F., et al. (2018). *PQR309* is a novel dual PI3K/mTOR inhibitor with preclinical antitumor activity in lymphomas as a single agent and in combination therapy. *Clin. Cancer Res.* **24**, 120–129.
- Vantourout, P., and Hayday, A. (2013). Six-of-the-best: unique contributions of gammadelta T cells to immunology. *Nat. Rev. Immunol.* **13**, 88–100.
- Vantourout, P., Laing, A., Woodward, M.J., Zlatareva, I., Apolonia, L., Jones, A.W., Sniijders, A.P., Malim, M.H., and Hayday, A.C. (2018). Heteromeric interactions regulate butyrophilin (BTN) and BTN-like molecules governing gammadelta T cell biology. *Proc. Natl. Acad. Sci. U S A* **115**, 1039–1044.
- Vavassori, S., Kumar, A., Wan, G.S., Ramanjaneyulu, G.S., Cavallari, M., El Daker, S., Beddoe, T., Theodossis, A., Williams, N.K., Gostick, E., et al. (2013). Butyrophilin 3A1 binds phosphorylated antigens and stimulates human gammadelta T cells. *Nat. Immunol.* **14**, 908–916.
- Viken, M.K., Blomhoff, A., Olsson, M., Akselsen, H.E., Pociot, F., Nerup, J., Kockum, I., Cambon-Thomsen, A., Thorsby, E., Undlien, D.E., et al. (2009). Reproducible association with type 1 diabetes in the extended class I region of the major histocompatibility complex. *Genes Immun.* **10**, 323–333.
- Wang, Q., Ding, H., He, Y., Li, X., Cheng, Y., Xu, Q., Yang, Y., Liao, G., Meng, X., Huang, C., et al. (2019). *NLR5* mediates cell proliferation, migration, and invasion by regulating the Wnt/beta-catenin signalling pathway in clear cell renal cell carcinoma. *Cancer Lett.* **444**, 9–19.
- Williams, G.S., Malin, M., Vremec, D., Chang, C.H., Boyd, R., Benoist, C., and Mathis, D.

(1998). Mice lacking the transcription factor CIITA—a second look. *Int. Immunol.* *10*, 1957–1967.

Wu, C., Orozco, C., Boyer, J., Leglise, M., Goodale, J., Batalov, S., Hodge, C.L., Haase, J., Janes, J., Huss, J.W., 3rd, et al. (2009). BioGPS: an extensible and customizable portal for querying and organizing gene annotation resources. *Genome Biol.* *10*, R130.

Yao, Y., Wang, Y., Chen, F., Huang, Y., Zhu, S., Leng, Q., Wang, H., Shi, Y., and Qian, Y. (2012).

NLRC5 regulates MHC class I antigen presentation in host defense against intracellular pathogens. *Cell Res.* *22*, 836–847.

Yoshihama, S., Roszik, J., Downs, I., Meissner, T.B., Vijayan, S., Chapuy, B., Sidiq, T., Shipp, M.A., Lizee, G.A., and Kobayashi, K.S. (2016). NLRC5/MHC class I transactivator is a target for immune evasion in cancer. *Proc. Natl. Acad. Sci. U S A* *113*, 5999–6004.

Zhu, L., and Jones, P.P. (1990). Transcriptional control of the invariant chain gene involves promoter and enhancer elements common to

and distinct from major histocompatibility complex class II genes. *Mol. Cell. Biol.* *10*, 3906–3916.

Zocchi, M.R., Costa, D., Vene, R., Tosetti, F., Ferrari, N., Minghelli, S., Benelli, R., Scabini, S., Romairone, E., Catellani, S., et al. (2017). Zoledronate can induce colorectal cancer microenvironment expressing BTN3A1 to stimulate effector gammadelta T cells with antitumor activity. *Oncoimmunology* *6*, e1278099.

Supplemental Information

NLRC5 promotes transcription of *BTN3A1-3* genes and V γ 9V δ 2 T cell-mediated killing

Anh Thu Dang, Juliane Strietz, Alessandro Zenobi, Hanif J. Khameneh, Simon M. Brandl, Laura Lozza, Gregor Conradt, Stefan H.E. Kaufmann, Walter Reith, Ivo Kwee, Susana Minguet, Sonia T. Chelbi, and Greta Guarda

Supplemental Information

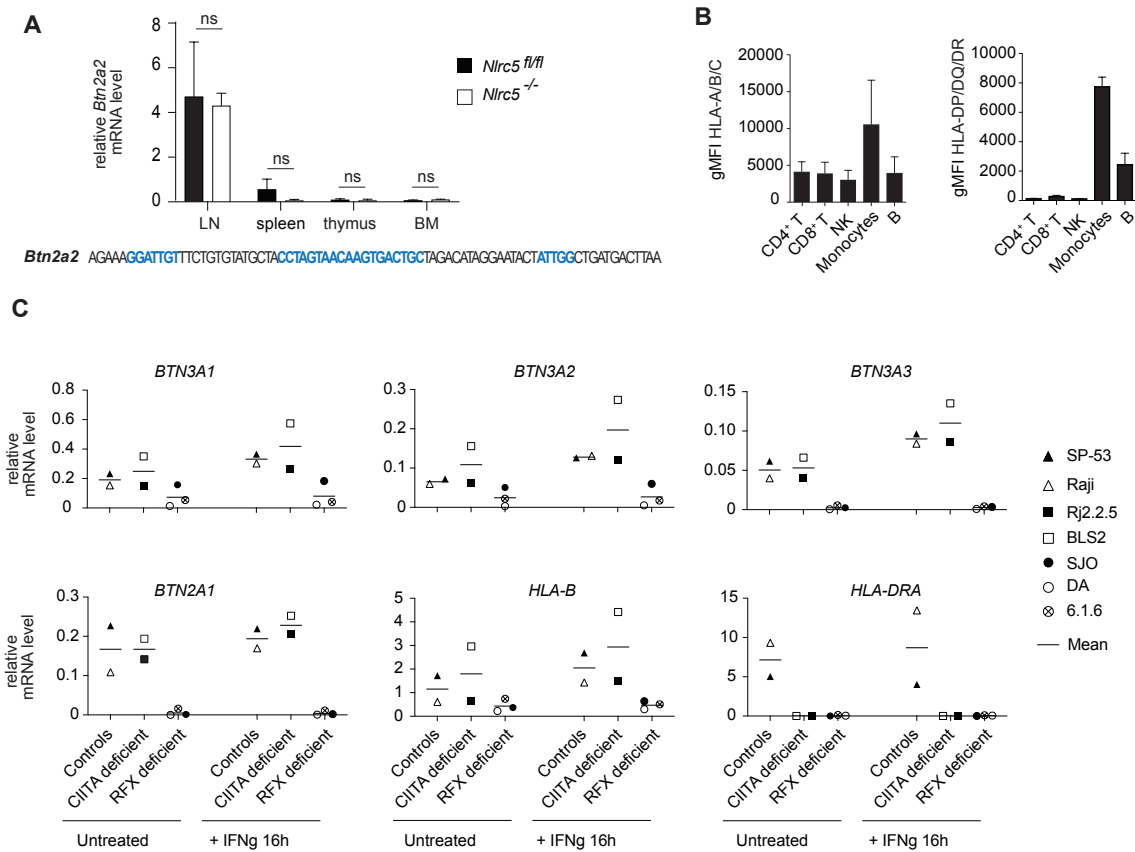


Figure S1. *BTN3A1*, *A2* and *A3* mRNA is not decreased in CIITA-deficient cell lines (related to Figure 1). (A) Murine *Btn2a2* promoter sequence and mRNA levels (relative to *Polr2a* mRNA) as assessed by quantitative RT-PCR (qRT-PCR) in lymph node (LN), spleen, thymus, and bone marrow (BM) of *Nlrc5^{fl/fl}* and *Nlrc5^{-/-}* mice. (B) Geometric mean fluorescence intensity (gMFI) of HLA-A/B/C and HLA-DR/DQ/DP as measured by flow cytometry in the indicated blood-derived cell subsets. (C) *BTN3A1*, *A2* and *A3*, *BTN2A1*, *HLA-B*, and *HLA-DRA* mRNA levels (relative to *POLR2A* mRNA) were measured by qRT-PCR in B cell-derived cell lines not expressing CIITA (Rj2.2.5; black square, BLS-2; white square), RFX5 (SJO; black circle), or RFXAP (DA; white circle, 6.1.6; white circle with cross) or controls (SP-53; black triangle, Raji; white triangle) treated or not with IFN γ for 16 hours. Results depict the mean \pm SEM of n=3 mice per genotype and are representative of two independent experiments (A), the mean \pm SEM of n=3 individual donors (B), or the mean of n=2 or n=3 cell lines, each represented as the average of n=3 independent measurements (C). (A) Statistical differences between genotypes were calculated using unpaired Student's t-test, two-tailed, unequal variance; ns: non significant.

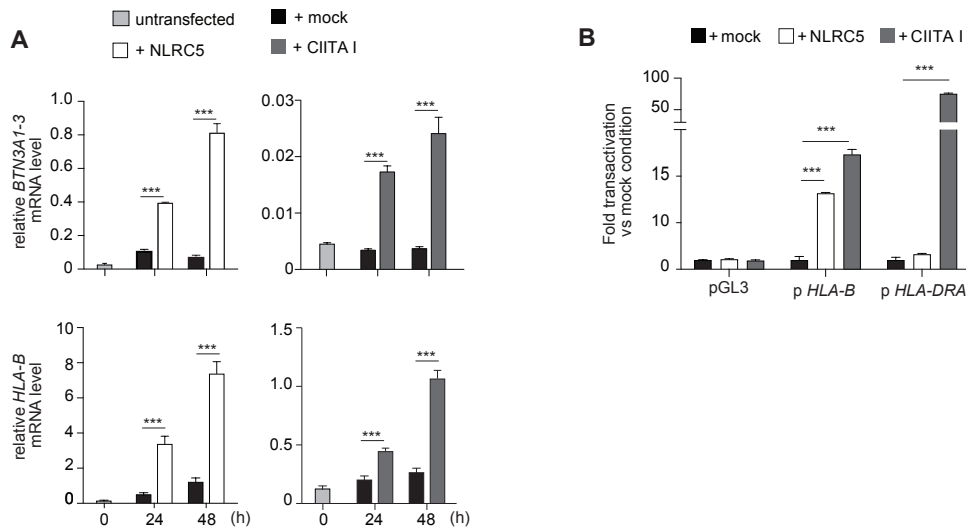


Figure S2. Overexpressed CIITA transactivates MHC class II and class I promoters (related to Figure 2). (A) *BTN3A1-3* and *HLA-B* mRNA levels (relative to *POLR2A* mRNA) were measured by qRT-PCR at basal ($t=0$ h, untransfected) and 24 h and 48 h following transfection of plasmids encoding the indicated NLR proteins or an empty vector (mock) in HEK293T. Results are depicted as mean \pm SD ($n=3$ technical replicates) and are representative of at least 2 independent experiments. Statistical differences were determined by two-way ANOVA followed by comparison of the experimental conditions to the corresponding mock transfection, and were corrected for multiple testing using the Holm-Sidak method. (B) Luciferase reporter assays were performed in HEK293T cells co-transfected with the parental pGL3 backbone, *HLA-DRA*, or *HLA-B* promoter constructs (reporters), and a vector coding for NLRC5, CIITA I, or an empty (mock) vector. Data are expressed as fold transactivation to the mock condition. Results represent mean \pm SD of $n=3$ technical replicates and are representative of at least three independent experiments. Statistical differences were determined by performing a two-way ANOVA followed by comparison of the experimental conditions to the corresponding mock transfection and were corrected for multiple testing using the Dunnett method. *** $p<0.001$. Only statistically significant differences are illustrated.

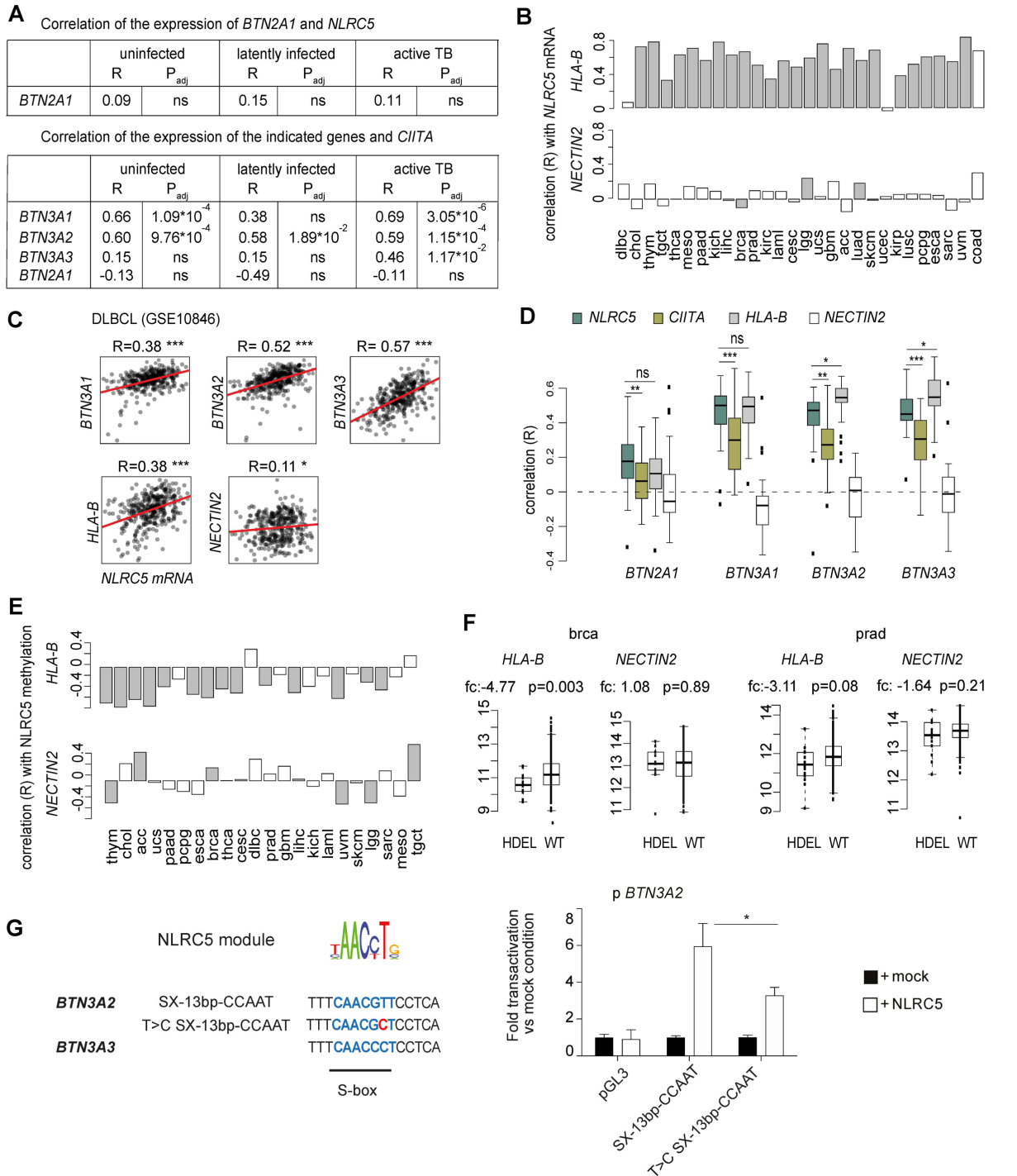


Figure S3. *NLRC5* mRNA correlates with *HLA-B* transcript abundance (related to Figure 6). (A) Pairwise correlation of *NLRC5* and *BTN2A1* and of *CIITA* and *BTN3A1*, *BTN3A2*, *BTN3A3*, *BTN2A1* expression were analyzed using transcriptome datasets of Gambia *M. tuberculosis* (TB) cohort study (GSE28623). The samples are divided in the groups 'uninfected', 'latently infected', and 'active TB'. The table displays the Spearman's correlation coefficient (R), and Bonferroni adjusted p-values (P_{adj}) for the 3 groups. (B, D-F) Data from The Cancer Genome Atlas (TCGA) provisional dataset collections were analyzed after adjustment for CD45 expression. (B) Spearman's correlation coefficient (R) for *NLRC5* and *HLA-B* or *NECTIN2* mRNA expression across cancer

types (C). Data from GSE10846 lymphoma dataset were analyzed after adjustment for CD45 expression. Scatterplots for *NLRC5* and *BTN3A1*, *BTN3A2*, *BTN3A3*, *HLA-B*, or *NECTIN2* mRNA expression are shown. Spearman's correlation coefficients (R) are indicated and significance was determined using the Bonferroni method. (D) Box plot depicting Spearman's correlation coefficient (R) distribution for the indicated *BTN* genes and *NLRC5*, *CIITA*, *HLA-B*, or *NECTIN2* mRNA expression across all cancers. Two group comparisons were performed using unpaired t-tests, two-tailed, unequal variance. (E) Spearman's correlation coefficient for *NLRC5* promoter methylation and *HLA-B* or *NECTIN2* mRNA expression across cancer types. (F) *HLA-B* and *NECTIN2* mRNA abundance is plotted according to *NLRC5* copy number status. fc: fold change of expression in HDEL (n=14 and n=13 for brca and prad, respectively) over WT group (n=272 and n=361 for brca and prad, respectively). HDEL: homozygous deletion; WT: wild type. Two group comparisons were performed using unpaired t-tests, two-tailed, unequal variance, and p-values are indicated. (G) Luciferase reporter assays were performed in HEK293T cells co-transfected with the parental pGL3 backbone or the indicated *BTN3A2* promoter constructs, and a vector coding for *NLRC5* or an empty (mock) vector. In the "T>C SX-13bp-CCAAT" construct, the T position was mutated into a C (in red) to resemble the S-box sequence found in the *BTN3A3* promoter. Data are expressed as fold transactivation as compared to the mock condition. Results represent mean \pm SD of n=4 technical replicates and are representative of 2 independent experiments. Statistical differences were determined by performing a two-way ANOVA followed by comparison of the SX-13bp-CCAAT to the T>C SX-13bp-CCAAT condition and were corrected for multiple testing using the Holm-Sidak method. * p<0.05, **p<0.01, *** p<0.001, ns: not significant. (B, E) Grey bars indicate significant correlation (p<0.05 after Bonferroni correction), white bars non-significant ones.

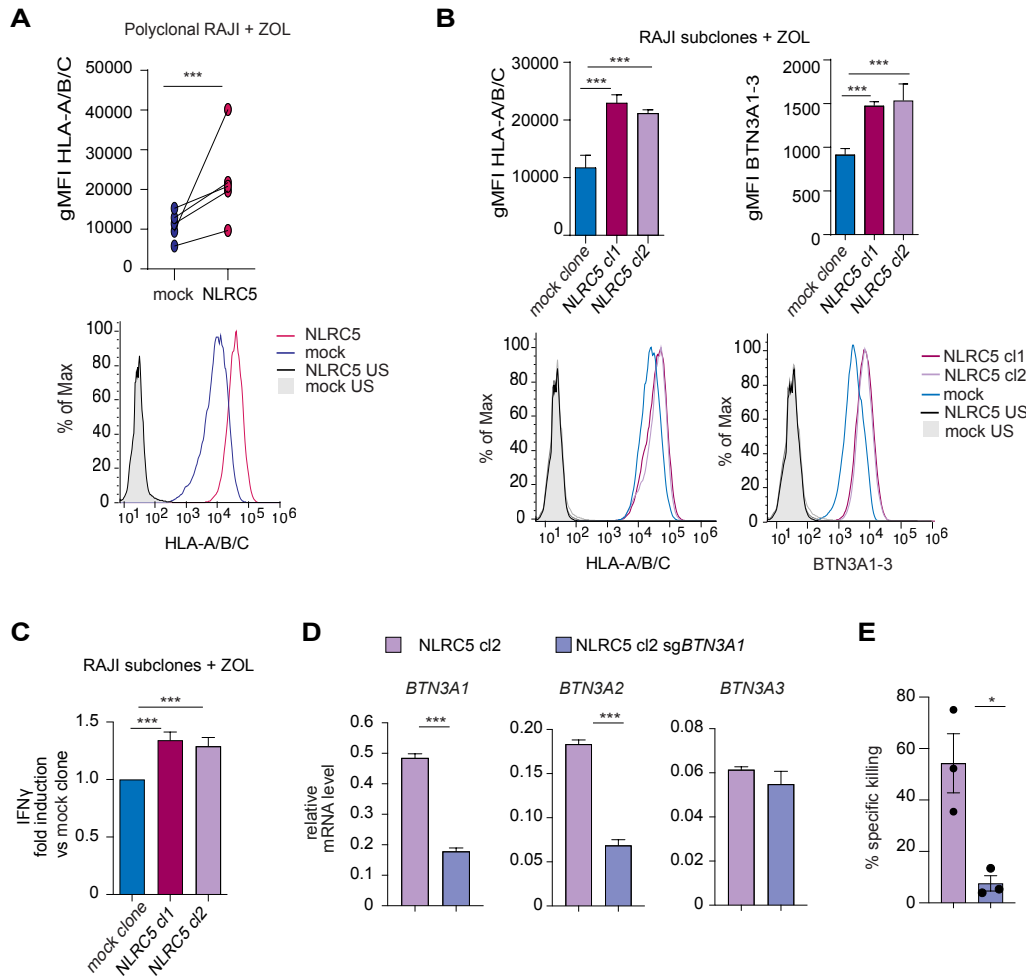


Figure S4. NLRC5 overexpression increases *BTN3A1-3* and *HLA-A/B/C* expression in Raji cells (related to Figure 7). (A) Polyclonal Raji cells were transduced with NLRC5 or empty vector (mock) and treated with zoledronate (ZOL) for 24 h. *HLA-A/B/C* surface expression was analyzed by flow cytometry. Graphs depict a quantification of *HLA-A/B/C* geometric MFI (gMFI; top) and histogram overlays (bottom) show *HLA-A/B/C* expression for unstained (US; black, grey), mock- (blue) and NLRC5-transduced polyclonal Raji cells (pink). Results represent 5 independent measurements. (B) Subclones were generated from Raji cells transduced with NLRC5 or empty vector (mock) and treated with ZOL for 24 h before *BTN3A1-3* and *HLA-A/B/C* surface expression was analyzed by flow cytometry. Graphs depict a quantification of *BTN3A1-3* and *HLA-A/B/C* gMFI (top) and histogram overlays (bottom) show *BTN3A1-3* and *HLA-A/B/C* expression for unstained (US; black, grey), mock- (blue) and NLRC5-transduced Raji subclones (red, violet). (C) IFN γ production by V γ 9V δ 2 T cells was measured after 48 h of co-culture with the mock - or the two NLRC5-transduced subclones at an effector-to-target ratio of 10:1 in the presence of ZOL. Results are depicted as IFN γ fold induction in presence of NLRC5-transduced as compared to the mock-transduced subclones. (D, E) *BTN3A1* was targeted by CRISPR/Cas9 in the NLRC5-transduced Raji subclone 2 (NLRC5 cl2 sg*BTN3A1*). NLRC5 cl2 and NLRC5 cl2 sg*BTN3A1* were assessed for *BTN3A1*, *A2*, and *A3* mRNA levels (relative to *POLR2A* mRNA) by qRT-PCR (D) and for their susceptibility to V γ 9V δ 2 T cell-mediated killing after 24 h of co-culture at an effector-to-target ratio of 10:1 in the presence of ZOL (E). Results are depicted as mean \pm SEM of n=3 independent measurements (B) as mean \pm SEM of n=4 healthy donors (C), as mean \pm SD of n=3 technical replicates (D), or as mean \pm SEM of n=3 healthy donors (E). Results are representative of at least 2 independent experiments (A-E). Statistical differences between the condition with and without NLRC5 overexpression were calculated using paired Student's t-test, two-tailed, unequal variance (A), by one-way ANOVA followed by comparison of the experimental conditions to the corresponding mock condition and were corrected for multiple testing using the Dunnett method (B, C), or by unpaired (D) or paired (E) Student's t-test, two-tailed, unequal variance. *p<0.05, ***p<0.001. Only statistically significant differences are illustrated.

Transparent Methods

Mice

Sex- and age-matched 6- to 12-week-old *Nlrc5^{fl/fl}* and *Nlrc5^{-/-}* (Stahli et al., 2012) mice on a C57BL/6 (H2^b) background were housed at the animal facility of the University of Lausanne. All animal experimental protocols were approved by the Veterinary office regulations of the State of Vaud, Switzerland, and all methods were performed in accordance with the Swiss guidelines and regulations.

Cell lines and transfections

HEK293T cells were cultured using DMEM high glucose supplemented, whereas the B-cell lines SP-53, Raji, Rj2.2.5, BLS-2, SJO, DA, and 6.1.6 (previously described in (Ludigs et al., 2015; Tarantelli et al., 2018)) were cultured in RPMI 1640 medium (Life Technologies) containing at least 10 mM HEPES. Culture media were all supplemented with GlutaMAX (2 mM), sodium pyruvate (1 mM), 10% fetal calf serum (FCS), 100 U/ml penicillin and 100 µg/ml streptomycin. For HEK293T cells, 0.1 mM MEM Non-essential Amino Acids (NEAA) were added in some experiments. Cells were incubated at 37°C in 5% CO₂. For transfection, HEK293T cells were subconfluently seeded and transfected the following day using PEI reagent (1.5:1 up to 3:1 PEI: DNA ratio) and harvested at the indicated time point for analysis.

Quantitative RT-PCR and sample preparation

To assess expression in human immune tissues, cDNA included in the “Human immune system MTC™ panel” (TAKARA) were used (pool from at least 9 individuals). Peripheral blood mononuclear cells (PBMC) were isolated by density centrifugation over a Ficoll-Hypaque

gradient (LymphoPrep) from blood of healthy human donors. Total PBMCs were surface stained with CD4⁺ T, CD8⁺ T, NK, monocyte and B cell markers, and sorted by flow cytometry using FACSria III sorter (BD Biosciences) as CD4⁺CD3⁺, CD8⁺CD3⁺, CD56⁺CD3⁻ CD14⁺, and CD19⁺ cells, respectively. Immune organs were collected and processed from *Nlrc5^{fl/fl}* and *Nlrc5^{-/-}* mice. RNA from cell lines, PBMC subsets, and murine lymphoid tissues was extracted using TRIzol® reagent (Ambion, Life Technologies) according to manufacturer's instructions. Annealing with random primers (Life Technologies) was performed at 70 °C for 5 min, followed by retrotranscription to cDNA with M-MLV RT, RNase H(-) point mutant (Promega), in presence of buffer, nucleotides (Roche Diagnostics), and RNasin® Plus RNase Inhibitor (Promega). Reaction was incubated at 40 °C for 10 min, 45 °C for 50 min and 70 °C for 15 min. cDNAs were diluted and quantitative PCR was performed using the LightCycler 480 SYBR Green I Master (Roche Diagnostics) on a LightCycler 480 machine (Roche Diagnostics). Expression was determined relative to *POLR2A*. Data were analyzed, and transcript abundance (gene/*POLR2A*) and s.d. were calculated using the LightCycler 480 software. Primers (Fwd; Rev) used were as follows: *Polr2a*: (5'-CCGGATGAATTGAAGCGGATGT-3'; 5'-CCTGCCGTGGATCCATTAGTCC-3'); *Btm2a2*: (5'-TAGGGGTCTCTCCACACAGC-3'; 5'-TATGACCAGGCAACCATGAA-3'); *POLR2A*: (5'-CGCACCATCAAGAGAGTCCAGTTC-3'; 5'-GTATTTGATGCCACCCTCCGTCA-3'); *BTN3A1-3*: (5'-ATGAAAAGCCCTGGTGGAG-3'; 5'-TGTATTTGGGGTTGGGGTA-3'); *HLA-B*: (5'-CTACCCTGCGGAGATCA-3'; 5'-ACAGCCAGGCCAGCAACA-3'); *HLA-DRA* : (5'-GCCAACCTGGAAATCATGACA-3'; 5'-AGGGCTGTTTGTGAGCACA-3'); *BTN2A1* : (5'-TGCTCGGCCAGAAGAAAGAA-3'; 5'-CCACAATGATAGGCAGGGC-3'); *BTN3A1*: (5'-CTTCAGCTGCTCATGCCTCA-3'; 5'-CAGATCAGCGTCTTCACCCA-3'); *BTN3A2* : (5'-

CAGTACTTGACTCGTGGAGAG-3'; 5'-TCAGGCTGACTTATTGGTATCGG-3'); *BTN3A3* : (5'-TCGTGGAGAGAAGTCTTTGG-3'; 5'-ACATCCGCAGGTTTGAAGA-3'); *NLRC5* : (5'-GTGCCTCTGGACCTGGAG-3'; 5'-GAGATTCAGGTTGGCTTTTCC-3'); *CIITA* : (5'-AGCCAAGTCCCTGAAGGATG-3'; 5'-TCTTAAGGTCCCGAACAGCAG-3').

Flow Cytometry

For flow cytometry analysis, sorted PBMCs or cell lines were surface stained using antibodies against HLA-A/B/C (W6/32, eBioscience or BioLegend), HLA-DP/DQ/DR (Tu39, BioLegend) and BTN3A1-3/CD277 (BT3.1, BioLegend or Miltenyi Biotec). Data were acquired using a FACS Canto (Becton Dickinson) or a Gallios (Beckman Coulter) flow cytometer and analyzed with FlowJo software (LCC, Becton Dickinson).

Plasmids and constructs

NOD1, NOD2, NLRC3 expression plasmid were obtained from the laboratory of the late J. Tschoop. CD72 expression plasmid was a kind gift from M. Thome-Miazza (UNIL, Switzerland). HLA-B170 (referred as p *HLA-B*) luciferase reporter plasmid was kindly provided by P.J. van den Elsen (Leiden University, Netherlands). HLA-DRA luciferase reporter and CIITA I/III expression plasmids were kindly gifted by W. Reith (UNIGE, Switzerland). For overexpression experiments, a NLRC5 encoding plasmid previously described was used (Stahli et al., 2012). For CHIP assays, a plasmid encoding NLRC5 in frame with a N-terminal HA-tag, referred here as wt NLRC5, has been generated. ORF was amplified using the KAPA Hifi PCR kit (KAPA Biosystems) using NLRC5 containing plasmid as template. PCR primers were extended with KpnI or XhoI restriction sites for oriented cloning into the pCMV-HA backbone.

NLRC5 Walker A domain mutant (K234A), named as mt NLRC5, was generated by site directed point mutagenesis using the wt NLRC5 construct as template. The pHRSIN-CS-Luc-IRES-emGFP plasmid was a kind gift from A. Rodriguez (UAM, Spain). The pHRSIN-CS-IRES-mTagBFP2 was generated by removing the luciferase and substituting the emGFP for the mTagBFP2 in the pHRSIN-CS-Luc-IRES-emGFP plasmid using the Gibson assembly cloning method. The lentiviral construction pHRSIN-CS-HA-NLRC5-IRES-mTagBFP2 coding for NLRC5 was generated by Gibson assembly using the pHRSIN-CS-IRES-mTagBFP2 as recipient plasmid and the HA-NLRC5 insert PCR amplified from the wt NLRC5 plasmid. Lentiviral packaging plasmids pCMVDR8.74 and pMD2.G were a gift from D. Trono (EPFL, Switzerland). Luciferase reporter plasmids were created by replacing the MluI-BglII fragment spanning the HLA-DRA SXY region in the pDRAprox plasmid (Krawczyk et al., 2004) with *BTN3A* promoter regions. Inserts were obtained either by PCR amplification using the GoTaq polymerase (Promega) or using annealed purchased DNA oligos (Microsynth AG). The pGL3 plasmid containing the remaining HLA-DRA core promoter (from -60 to +10) in the same reporter plasmid was used as negative control. All generated constructs were verified by sequencing. Sequences of primers used for cloning are available upon request.

Luciferase reporter assay

HEK293T cells were seeded into a 96-well plate and transfected the following day using PEI reagent with human NLRC5, or human CIITA I expression vectors, or an empty backbone as control (mock), and the indicated luciferase reporter constructs. The pRLTK (Renilla) luciferase reporter was included for normalization. Cells were harvested between 20 and 30 h post-transfection and cell lysates were analyzed using the Dual-Luciferase® Reporter Assay System

(Promega) following manufacturer's instruction. Bioluminescence was measured using the Enspire™ Alpha2390 Multilabel Reader (PerkinElmer).

Chromatin immunoprecipitation (ChIP)

HEK293T cells were transiently co-transfected with plasmids encoding for HA-tagged human NLRC5 (wt NLRC5) or human NLRC5 Walker A mutant (mt NLRC5) and human CD72. After 48 h, cells were collected and stained with FITC-labeled α -CD72 (3F3; BioLegend) followed by incubation with α -FITC magnetic beads for MACS enrichment (Miltenyi Biotech). Chromatin was prepared from CD72⁺ cells as previously described (Masternak et al., 2003). Immunoprecipitation was performed using a ChIP grade anti-HA tag antibody (ab91110, Abcam). Analysis of specific DNA regions was performed by quantitative PCR. The amount of immunoprecipitated DNA was calculated from the standard curves generated with the input chromatin and fold enrichment was determined relative to the mt NLRC5 condition. The promoter of *HOXC8*, which is not a NLRC5 target, is used as negative control. Primers (Fwd; Rev) are listed hereafter: *BTN3A1*: (5'- GGGAGGTAGGGCAGGAATTT -3'; 5'- CACTGAGGAAGGCTGAAATGA-3'); *BTN3A2*: (5'- TGAGAAACATCACCTCTGAGCCA; 5'- CCATGAGAAACAGTAAGAGTCGC-3'); *HLA-B*: (5'- GTGTCGGGTCCTTCTTCCA-3'; 5'- CCAATGGGAGTGGGAAGTG-3'); *HOXC8*: (5'-CTCAGGCTACCAGCAGAACC-3'; 5'- TTGGCGGAGGATTTACAGTC-3').

Generation of Raji target cells for cytotoxicity assays

To produce lentiviral particles HEK293T cells were co-transfected with the pCMVDR8.74 and pMD2.G packaging vectors, the pHR SIN-CS-Luc-IRES-emGFP plasmid encoding for the

luciferase, and either the pHRSIN-CS-HA-NLRC5-IRES-mTagBFP2 construct expressing NLRC5 or the empty pHRSIN-CS-IRES-mTagBFP2 as control (mock). After transduction, Raji cells double positive for mBFP2 and luciferase expression were isolated using the MoFlo Astrios cell sorter (Beckman Coulter) and were used for the cytotoxicity assays as polyclonal population. To obtain Raji subclones, single-cell subcloning was performed using limiting dilution of the polyclonal Raji cells. In this context, culture medium was supplemented with 2- β -mercaptoethanol (0.05 mM).

CRISPR/Cas9-mediated gene disruption of BTN3A1 was conducted with a combination of two pre-designed chemically stabilized Alt-R CRISPR-Cas9 crRNAs (crRNA XT; IDT) and the Alt-R CRISPR Cas9 system of Integrated DNA Technologies. For duplex formation, the chemically stabilized crRNAs XT Hs.Cas9.BTN3A1.1.AL (5'-ACCAUCAGAAGUUCCCUCCU-3', IDT) and Hs.Cas9.BTN3A1.1.AP (5'-GAUGUGAAGGGUACAAGGA-3', IDT) were mixed in equimolar amounts with Alt-R CRISPR-Cas9 tracrRNA (IDT) to a final oligo concentration of 44 μ M, heated to 95°C for 5 min and cooled down to RT for gRNA duplex formation (crRNA XT:tracrRNA). Alt-R S.p. Cas9 Nuclease V3 protein (IDT) was used at 36 μ M. For ribonucleoprotein (RNP) assembly, the gRNA duplex was mixed with Alt-R S.p. Cas9 Nuclease V3 protein at equal volumes and incubated for 20 min at RT. RNP complexes were then stored on ice prior utilization. Electroporation of Raji cells was conducted with the Neon Transfection System (Invitrogen, Life Technologies, 1 pulse of 1,350 V for 30 ms) and in the presence of Alt-R Cas9 Electroporation Enhancer (10.8 μ M; IDT). Cells were then transferred into pre-warmed complete medium and incubated at 37°C and 5% CO₂.

Expansion of human V γ 9V δ 2 T cells and cytotoxicity assays

Human V γ 9V δ 2 T cells were expanded from human PBMCs isolated from healthy donors using a Ficoll-Hypaque gradient. Cells were cultured in RPMI 1640 medium + GlutaMAX (Life Technologies) supplemented with 10% fetal calf serum (FCS), 50 U/ml penicillin, 50 μ g/ml streptomycin, 10 mM HEPES buffer, 1 mM sodium pyruvate and 1x MEM non-essential amino acid solution. For $\gamma\delta$ T cell expansion, PBMCs were stimulated either with 2.5 μ M zoledronate and 50 U/ml rIL-2 or with 1 μ g/ml concanavalin A and 10 ng/ml rIL-2 and 10 ng/ml rIL-4. For zoledronate expanded V γ 9V δ 2 T cells, fresh rIL-2 was added every second day over a culture period of 21 days. After 7 days, the expanded V γ 9V δ 2 T cells were additionally split at a 1:2 ratio every second day. 14 days after stimulation, the purity of the expanded V γ 9V δ 2 T cells was evaluated by flow cytometry and cells were MACS-enriched if required (TCR γ/δ + T Cell Isolation Kit, human, Miltenyi Biotech). For bioluminescence-based killing assays, 10,000 luciferase-expressing NLRC5- or mock-transduced Raji cells were co-cultured with either 10,000 (1:1), 50,000 (5:1) or 100,000 (10:1) expanded V γ 9V δ 2 T cells in triplicates for 24 h at 37°C and 5% CO₂ in the presence of 10 μ M zoledronate. The proportion of living cells was measured as bioluminescence in relative light units (RLU) at an Infinite 200 PRO plate reader (Tecan) in the presence of the substrate D-firefly luciferin potassium salt (37.5 μ g/ml, Biosynth). Specific killing was calculated relative to Raji cells treated either with medium alone (spontaneous death) or with 1% Triton X-100 (maximal death) with the following formula: % specific killing = 100 x (average spontaneous death RLU - test RLU) / (average spontaneous death RLU - average maximal death RLU). Quantification of IFN γ production was performed by co-culturing 10,000 NLRC5- or mock-transduced Raji subclone cells with 100,000 V γ 9V δ 2 T cells (10:1) for 48 h in the presence of 10 μ M zoledronate, followed by standard enzyme linked immunosorbent assay (ELISA) from Invitrogen, Life Technologies.

Bioinformatic analyses of Gambia cohort and tumor datasets

We selected 32 TCGA cancer types from the TCGA provisional data set collections as available from cBioportal (June 2019). Genetic profiles for mRNA expression, methylation and copy number of selected genes were retrieved using the ‘cgdsr’ R/Bioconductor package. Adjustment for potential confounding factors (here CD45/PTPRC) was performed using the ‘removeBatchEffect’ function from the limma R/Bioconductor package using CD45 expression as covariate. For the independent diffuse large B-cell lymphoma (DLBCL) cohort, we downloaded gene expression data (GSE10846) from the NCBI GEO database using the ‘GEOquery’ R package, and corrected the data for CHOP/RCHOP treatment effects and for CD45 expression. Similarly, for the Gambia cohort, we downloaded the gene expression data (GSE28623) from GEO. For GSE10846 DLBCL, we used the 350 samples with ABC or GCB subtype and batch-corrected for chemotherapy. No batch correction or adjustment for CD45 was deemed to be needed. For continuous variables, statistical correlation and significance was assessed using Spearman’s correlation. For 2 group comparisons, the t-test (two-sided, unequal variance) was used to assess differences in means. Statistical analysis was performed using R version 3.5.2 and BioConductor 3.8 on Ubuntu/Linux. Cancer types are abbreviated according to the TCGA database (<https://gdc.cancer.gov/resources-tcga-users/tcga-code-tables/tcga-study-abbreviations>): dlbc: Lymphoid Neoplasm Diffuse Large B-cell Lymphoma; chol: Cholangiocarcinoma; thym: Thymoma; tgct: Testicular Germ Cell Tumors; thca: Thyroid carcinoma; meso: Mesothelioma; paad: Pancreatic adenocarcinoma; kich: Kidney Chromophobe; lihc: Liver hepatocellular carcinoma; brca: Breast invasive carcinoma; prad: Prostate adenocarcinoma; kirc: Kidney renal clear cell carcinoma; laml: Acute Myeloid Leukemia; cesc:

Cervical squamous cell carcinoma and endocervical adenocarcinoma; lgg: Brain Lower Grade Glioma; ucs: Uterine Carcinosarcoma; gbm: Glioblastoma multiforme; acc: Adrenocortical carcinoma; luad: Lung adenocarcinoma; skcm: Skin Cutaneous Melanoma; ucec: Uterine Corpus Endometrial Carcinoma; kirp: Kidney renal papillary cell carcinoma; lusc: Lung squamous cell carcinoma; pcp: Pheochromocytoma and Paranglioma; esca: Esophageal carcinoma; sarc: Sarcoma; uvm: Uveal Melanoma; coad: Colon adenocarcinoma.

Ethics

Mice were treated in accordance with the Swiss Federal Veterinary Office guidelines. For expression analyses, PBMCs were isolated from blood donations obtained from the Blood Transfusion Center, Switzerland. For experiments using V γ 9V δ 2 T cells, informed consent was obtained from the donors in accordance with the Declaration of Helsinki and Institutional Review Board approval from the University of Freiburg Ethics Committee (412/9). Human cell lines are established cell lines.

Statistical analysis

Statistical analyses were performed using either Prism software (GraphPad version 8.2.0) or R version 3.5.2 and BioConductor 3.8 on Ubuntu/Linux. For 2 group comparisons, t-tests (two-tail, unequal variance) were used to assess differences in means. In case of multiple testing, overall effects were determined by ANOVA and *post hoc* comparisons to the control condition were performed using either Dunnett's or Holm-Sidak method. For continuous variables, statistical correlation and significance was assessed using Spearman's correlation, Bonferroni method was

used to adjust for multiple correlations. Differences were considered significant when $P < 0.05$ (*), very significant when $P < 0.01$ (**) and highly significant when $P < 0.001$ (***)).